UNIVERZITA PALACKÉHO V OLOMOUCI

PŘÍRODOVĚDECKÁ FAKULTA

KATEDRA OPTIKY

MAGISTERSKÁ DIPLOMOVÁ PRÁCE

Experimenty s kvantovým zpracováním informace na bázi kvantové optiky

Autor: Bc. Helena Fikerová

Vedoucí práce: Prof. RNDr. Miloslav Dušek, Dr.

Studijní obor: Optika a optoelektronika

Olomouc 2014

PALACKÝ UNIVERSITY IN OLOMOUC

FACULTY OF SCIENCE

DEPARTMENT OF OPTICS

MASTER'S DIPLOMA THESIS

Quantum Optics-Based Experiments in Quantum Information Processing

Author: Bc. Helena Fikerová

Thesis supervisor: Prof. RNDr. Miloslav Dušek, Dr.

Study programme: Optics and Optoelectronics

Olomouc 2014

Prohlášení:

Prohlašuji, že jsem diplomovou práci „Experimenty s kvantovým zpracováním informace na bázi kvantové optiky“ vypracovala samostatně pod vedením prof. RNDr. Miloslava Duška, Dr. a s využitím zdrojů uvedených v seznamu literatury.

V Olomouci, 28. července 2014

Poděkování:

Ráda bych tímto poděkovala vedoucímu Prof. RNDr. Miloslavu Duškovi, Dr. za poskytnutý čas, pomoc a rady jak v experimentální tak i teoretické oblasti, trpělivé konzultace a pečlivé vedení této práce, Mgr. Martině Mikové za společnou práci na experimentu a neocenitelnou podporu a pomoc při psaní práce, Mgr. Miroslavu Ježkovi, Ph.D., Mgr. Ivovi Strakovi a Mgr. Michalu Mičudovi, Ph.D. za zásadní spolupráci při přípravě experimentu a Doc. Mgr. Radimu Filipovi, Ph.D. za přispění a rady v oblasti teorie.

Abstrakt

Cílem této diplomové práce byla experimentální realizace přenosu kvantového stavu pomocí protokolu využívajícího fotonové qubity, lineární optiku a jednofotonové detektory, jehož účelem bylo demonstrovat význam navrženého parametru efektivní nerozlišitelnosti v kvantovém zpracování informace. Experimentální uspořádání se zakládalo na dvou propojených vláknových Mach-Zehnderových interferometrech a využívalo qubitů kódovaných do prostorových modů fotonových párů generovaných parametrickou down-konverzí v nelineárním krystalu BBO. Přenos stavu se uskutečnil prohozením dvou ramen mezi interferometry a následným změřením jednoho z qubitů. Výsledný stav byl rekonstruován pomocí kvantové tomografie a spočtené veličiny prokázaly závislost kvality přenosu stavu na navrhovaném parametru nerozlišitelnosti. Výsledky byly publikovány ve Physical Review A.

Klíčová slova

Efektivní nerozlišitelnost, fotonové qubity, kvantové zpracování informace, teorie kvantové informace, vláknová optika, Mach-Zehnderův interferometer.

Abstract

The aim of this thesis was to experimentally implement a quantum state transfer protocol using photonic qubits, linear optics and single-photon detectors. The transfer protocol was used to demonstrate the relevance of the proposed quantitative measure of effective indistinguishability for quantum information processing. The experimental setup was based on two intertwined fibre Mach-Zehnder interferometers and used qubits encoded into spatial modes of photon pairs generated by spontaneous parametric down-conversion in a BBO crystal. The transfer was realized by means of swapping two rails between the interferometers and subsequent measurement on one of the qubits. The output state was reconstructed by means of maximum-likelihood quantum state tomography and dependence of the quality of state transfer on the indistinguishability parameter proposed was successfully proven. Results were published in Physical Review A.

Keywords

Effective indistinguishability, photonic qubits, quantum information processing, quantum information theory, fibre optics, Mach-Zehnder interferometer.

Contents

Introduction

This Master's thesis primarily falls into the area of experimental optical quantum information processing. The aim of the thesis was to experimentally implement a transfer protocol that would transfer a quantum state from a source onto a target photon and in this way carry out a partial exchange of their environmental basis states. The protocol was then applied to test the theoretical concept of a quantitative measure of effective indistinguishability defined by means of a flip operator acting on the joint environment of the photons. It was demonstrated that the quality of the quantum state transfer depended directly on the measure of effective indistinguishability proposed even when the particles were entangled. Hence, in the big picture, this experiment has investigated the effect of particle distinguishability on the processing of information and proposed a generally valid operational measure of effective indistinguishability.

Indistinguishability of particles is an important resource in many quantum information processing and communication tasks that have been devised up to this date. However, before the realization of the experiment described here, only a measure valid for factorable states had been developed. As indistinguishability might be required along with entanglement, e.g. in quantum teleportation and quantum protocols using the interference of two entangled photons, the quantitative measure proposed for the sake of this experiment is valid for an arbitrary state. The setup employed eliminated the influence of other resources to demonstrate its relevance in quantum information processing. In more complex setups, however, the quality of information processing might depend on other factors as well.

The results of the experiment were published in Physical Review A [1]. The core of my work lied in preparing the setup for computer-run measurement and the programming of this measurement, in particular a method of effective stabilization of the experiment. The following text shortly introduces the field of optical quantum information processing, provides a general theoretical background and reports the experiment. First, the physics underlying the experimental setup is explained, then a more detailed description of the technical implementation is given and finally, results are presented and analysed.

1 Motivation

1.1 Quantum Computing and Quantum Information Processing

Quantum computing and information processing is a modern field of research concerned with using and profiting from quantum mechanical systems for the encoding and processing of information and devising applicable technology that would allow this. The main motivation behind employing quantum mechanics in computing and communication is both historical and practical. In the historical perspective, the development of the field has been connected to the problem of computer power. Along with the technological development in classical computation, researchers have been investigating the theoretical limits of computer performance. Those problems that could be efficiently, that is, with computing time growing in a polynomial manner with respect to the size of the problem, solved on the model Turing machine, could also be solved by means of real hardware. However, the question arose of whether a different computational strategy might allow solving what could only be computed inefficiently by the classical model. In 1982, Richard Feynman showed that although the Turing machine would not be able to simulate a quantum system efficiently, a quantum computer could do so. David Deutsch generalized the idea three years later and looked for a computation model that would allow simulating any physical system; as physical systems are fundamentally quantum mechanical, he proposed a universal quantum computer. Since early 1980s, quantum computers have appeared to offer an important speed-up over classical computers. However, although increased speed was ascertained with certain problems, for example simulations of quantum mechanical systems and Shor's algorithms, we are still not capable of making a general comparison of the power of classical and quantum computational models as the advantage of quantum computers over the classical ones has not been proven. Nevertheless, research in quantum information processing has brought new important knowledge about quantum systems and continues to help our current understanding of quantum mechanics [2,3].

1.2 The Quantum Bit

Analogously to classical computers, the basic information carrier in quantum computing is the quantum bit. Whereas the classical bit can exist in one of two states: 0 or 1, the qubit

can exist in a superposition of two states $|0\rangle$and $|1\rangle$; its state can thus in general be expressed as:

$$|\psi\rangle = \alpha|0\rangle + \beta|1\rangle$$

whereα and β are complex numbers, that is, as a vector in 2-dimensional Hilbert space in which the states $|0\rangle$ and $|1\rangle$ form an orthonormal basis. However, if we measure the qubit, it will only be found in one of the two states $|0\rangle$ and $|1\rangle$ with corresponding probabilities $|\alpha|^2$and $|\beta|^2$and their superposition will be lost. This means that if we want to avail of superposition and at the same time find out what state the qubit is in, we cannot simply read the whole state; to process information, special quantum logical operations have to be devised to manipulate qubits while keeping their superpositions. As it holds for the probabilities that $|\alpha|^2$+ $|\beta|^2 = 1$, the state of the qubit can be conveniently transcribed as

$$|\psi\rangle = e^{i\eta}\big(\cos\omega\,|0\rangle + e^{i(\mu-\eta)}\sin\omega\,|1\rangle\big),$$

where η, ω and μ are real numbers and the overall phase factor $e^{i\eta}$ can be omitted as it has no physical significance. We can conveniently rewrite the state in the form

$$|\psi\rangle = \cos\frac{\theta}{2}|0\rangle + e^{i\phi}\sin\frac{\theta}{2}|1\rangle$$

which can be graphically depicted by means of the so-called *Bloch sphere*: the pure state of the qubit is represented by a point on the surface of this 3-dimensional sphere, given by the numbers θ and ϕ (see Fig. 1.1).

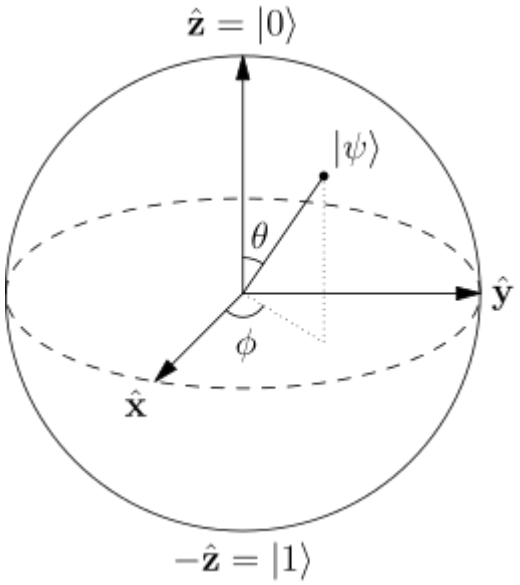

Fig. 1.1: The Bloch sphere. Source: wikipedia.org.

The qubit can be carried by an arbitrary two-level quantum system, for example, a photon existing in the superposition of two polarization or spatial modes [2,4].

1.3 Using Optics for QIP

Photons are good information carriers: they are not charged and almost do not interact with each other, show little decoherence, can efficiently be transported over long distances via optical fibres and are easily manipulated with phase shifters and beam splitters. Although logical gates require interaction, this can be mediated indirectly through photon detection. Direct interaction in non-linear media is also possible, but difficult to produce on a large enough scale; however, only linear quantum information processing is of interest here. Furthermore, photons readily exhibit interference and entanglement, key quantum phenomena that could be employed in optical quantum computing architecture [2,5,6].

Various encoding of information has been used with photons as qubit carriers. The basis states of an optical qubit can be represented, for example, by two different optical modes (the so-called *dual-rail* representation) as in the experiment described here, by two orthogonal polarization modes, temporal modes (the so-called time-bin encoding) or modes with different angular momenta [2,7]. Still, the possibility to encode information does not suffice by itself; the quantum computer has to be build out of a *universal* set of logical gates, that is, it has to be able to perform any desired computation on the quantum computer, which translates into performing an arbitrary unitary operation on a qubit [4]. Moreover, the logical protocols used have to be *scalable*: they should be efficient not only in solving small-scale problems, but also stay efficient and not fail when the amount of information to be processed increases [5,8]. In 2001, Knill, Laflamme and Milburn presented a linear optical scheme for efficient, scalable and universal optical quantum computation that could be implemented only with single photons, beam splitters, phase shifters and photon detectors [8]. Thus linear optical quantum computer architecture is possible in principle; it employs projective measurement to substitute for direct interaction and requires available technology.

A good approximation of a source of single photons is laser light that is composed of coherent states. Single photon sources can be constructed by attenuating the laser output so that it produces, with a very high probability, no photons at all and with a low probability

one photon at a time, so that the probability of two or more photons exiting the output in a unit of time is made approximately negligible. Alternatively, as it was done in this experiment, single photons can be generated via a non-linear medium and spontaneous parametric down-conversion (SPDC) [2,9]. SPDC is a non-linear optical process that takes place in non-linear crystals characterized by second-order non-linear susceptibility and in which the initial incoming photon is converted into two so-called idler and signal photons in the following manner:

$$\hat{a}_{inc}\hat{a}_i^{\dagger}\hat{a}_s^{\dagger}|1\rangle_{inc}|0\rangle_i|0\rangle_s = |0\rangle_{inc}|1\rangle_i|1\rangle_s$$

where $\hat{a}$ and $\hat{a}^{\dagger}$ are annihilation and creation operators respectively. The word spontaneous points at the quantum character of the process as the resulting modes are generated from vacuum states [10]. In addition, SPDC offers an effective way of producing photon pairs entangled in time, polarization or spatial modes via a careful selection of generated photons because the equation above is valid for a number of different modes and the state resulting from down-conversion is in general a superposition of the possible modes. SPDC is described in more detail in the following chapter.

2 Theoretical Framework

2.1 Operational Measure of Indistinguishability

Indistinguishability is an inherent feature of quantum particles. Even identical classical particles cannot be distinguished unless we follow their trajectory; however, this is not possible in quantum mechanics where we only have information about the probability of detecting the particle at a certain point in space and its trajectory cannot be followed without changing its state. In linear optical quantum information processing and communication, indistinguishability is a desirable quality which can influence considerably the performance of information protocols. Specifically, in such experiments, we are concerned with particles that are effectively indistinguishable, that is, particles that differ in those degrees of freedom in which we encode information and all their other internal degrees of freedom are identical. A certain measure of effective indistinguishability is therefore a helpful tool for operating with these particles.

If two particles are indistinguishable, the state of the total system has to be invariant to the exchange of the particle labels, more precisely, if ψ is the wave function of the total system,

$|\psi(\zeta_1, \zeta_2)|^2 = |\psi(\zeta_2, \zeta_1)|^2$,

ζ_1, ζ_2 denoting the different degrees of freedom of the particles, and therefore,

$\psi(\zeta_1, \zeta_2) = e^{i\varphi}\psi(\zeta_2, \zeta_1) \Rightarrow e^{2i\varphi} = 1.$

Indistinguishability thus introduces exchange symmetry into the system such that its wave function is symmetric or anti-symmetric with respect to the exchange of labels:

$\varphi = 0 \Rightarrow \psi(\zeta_1, \zeta_2) = +\psi(\zeta_2, \zeta_1)$ (bosons)

or$\varphi = \pi \Rightarrow \psi(\zeta_1, \zeta_2) = -\psi(\zeta_2, \zeta_1)$ (fermions) [11,12, 13].

Photons are bosons so their wave function or state vector is symmetric.

If we introduce a partial exchange operator, here called flip operator, F, that only exchanges some, here all non-informational, degrees of freedom of the particles, we can write for factorable environmental states of two particles labelled 1 and 2:

$F(\rho_1 \otimes \rho_2)F^\dagger = \rho_2 \otimes \rho_1.$

The mean value of the flip operator then equals the overlap of the two separable states:

$\langle F\rangle = Tr[F(\rho_1 \otimes \rho_2)] = Tr[\rho_1\rho_2]$.

However, as it was hinted on in the introduction, we are interested in a measure valid for arbitrary states as some degrees of freedom of the particles we use in our experiments can be entangled. Let us consider two identical qubits carried by two particles *S* (source) and *T* (target) and label the state of all their environmental degrees of freedom, except those that carry the qubits, $\rho_{E,ST}$ where *E* stands for environment. We thus define a measure of effective indistinguishability $|D|$ where *D* is a parameter that can be measured directly:

$D = Tr\left[F\rho_{E,ST}\right]$, (2.1)

and F_A is a flip operator:

$F_A = \sum_{m,n}|\psi_n\rangle_S\langle\psi_m| \otimes |\psi_m\rangle_T\langle\psi_n|$ (2.2)

that exchanges basis states with respect to an observable *A*. It is Hermitian and unitary:

$F_A = F_A^\dagger$ and $F_A F_A^\dagger = F_A^\dagger F_A = I$;

since it is invariant to the choice of operator *A*, we denote it *F* and deal with it here as effectively basis-independent. Furthermore, *F* can be expressed as a difference of orthogonal projectors onto the symmetric and anti-symmetric subspace of the total space:

$F = \Pi_{\text{sym}} - \Pi_{\text{antisym}}$,

which demonstrates its connection to the indistinguishability of the environmental states. Consequently, *F* has two eigenvalues ± 1 and $-1 \leq \text{Tr}[F\rho] \leq 1$, so

$-1 \leq D \leq 1$.

Identical local unitary transformations of the states of the two particles do not change *D*, it other words, do not influence indistinguishability. A symmetric state of two particles *S* and *T* such that $\rho_{E,ST} = F\rho_{E,ST} = \rho_{E,ST}F$ has $D = 1$ even if the particles are entangled [1].

2.2 Parametric Down-Conversion

2.2.1 Principle

The photon pairs we used in our experiment as source and target qubits were generated by spontaneous parametric down-conversion (SPDC) in a BBO (β-barium borate) crystal [9]. As

it was mentioned earlier, SPDC is a process occurring in non-linear media characterized by second-order nonlinear susceptibility $\chi^{(2)}$in which pump photons are converted into pairs of photons, commonly denoted signal and idler, of lower frequencies. Energy and momentum have to be conserved in the process; this translates into two, so-called "phase matching", conditions for the frequencies and the wave vectors of the three photons involved in the interaction (see Fig. 2.1 and 2.2):

$\omega_s + \omega_i = \omega_{pump}$

$\vec{k}_s + \vec{k}_i = \vec{k}_{pump}$

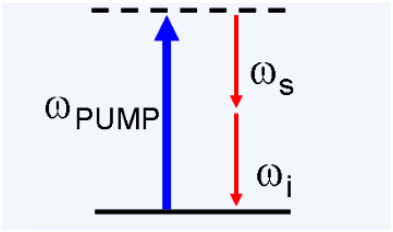

Fig. 2.1: Conservation of energy$E = \hbar\omega$. Source: wikipedia.org.

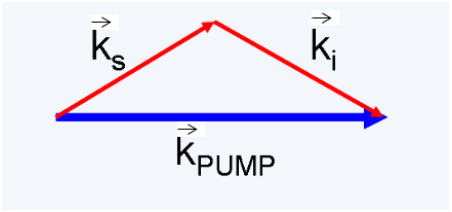

Fig. 2.2: Conservation of momentum $\vec{p} = \hbar\vec{k}$. Source: wikipedia.org.

As the refractive indices for different frequencies and momentum directions are in general different in dispersive and anisotropic crystals, the generated photons can in principle travel in different directions and the output state is a superposition of all the permitted possibilities which depends on the type of down-conversion. In type I SPDC, the directions of signal and idler photons form two concentric cones (see Fig. 2.3) and the generated photons have parallel polarization (orthogonal to that of the pump photon) and both travel as ordinary waves; in type II SPDC, they travel along two intersecting cones (see Fig. 2.4) and have orthogonal polarization, one as an ordinary, the other as an extraordinary

wave [3, 10]. The latter type is a valuable means of producing polarization-entangled photon pairs when directions where the cones intersect are selected using pinholes.

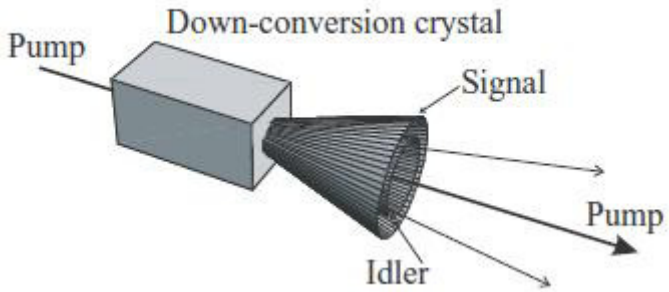

Fig. 2.3: Type I down-conversion. Source: [10].

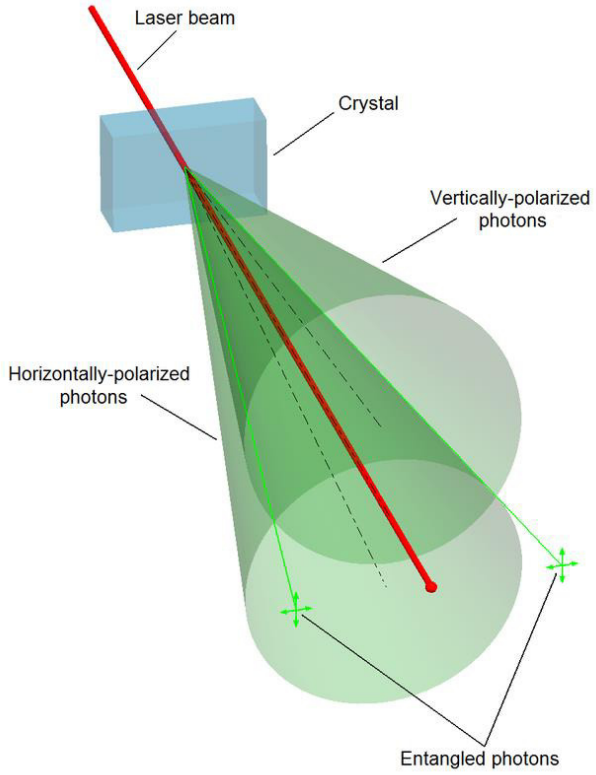

Fig. 2.4: Type II down-conversion. Source: wikipedia.org.

2.2.2 Theoretical Model

If we post-select two idler and signal directions that satisfy the phase matching conditions, the Hamiltonian for three-wave mixing can be expressed:

$$\widehat{H} = \sum_{i=1}^{2} \hbar\omega_i \left(a_i a_i^\dagger + \frac{1}{2}\right) + \hbar\omega_p \left(a_p a_p^\dagger + \frac{1}{2}\right) + \hbar g\left(a_1 a_2 a_p^\dagger + a_1^\dagger a_2^\dagger a_p\right)$$

where subscript *p* denotes the pump photons and g an interaction constant containing the susceptibility $\chi^{(2)}$. We suppose that the pump field is strong enough to be considered classical. It thus does not have to appear as quantized in the overall Hamiltonian and can be expressed as classical complex amplitude. The Hamiltonian can then be written:

$$\widehat{H} = \sum_{i=1}^{2} \hbar\omega_i \left(a_i a_i^{\dagger} + \frac{1}{2}\right) + \hbar g\left(a_1 a_2 v_p e^{-i\omega_p t} + h.c.\right)$$

The first term corresponds to the two mode field of idler and signal photons and the second to the interaction between the modes; this description is only valid for the mean generated number of photons $\ll |v_p|^2$. In the Heisenberg picture, the equations of motions yield the solutions [3, 14]

$$\hat{A}_1(t) = \hat{A}_1(0)\cosh\left(g.|v_p|.t\right) - ie^{i\vartheta}\hat{A}_2^{\dagger}(0)\sinh(g.|v_p|.t)$$

$$\hat{A}_2(t) = \hat{A}_2(0)\cosh\left(g.|v_p|.t\right) - ie^{i\vartheta}\hat{A}_1^{\dagger}(0)\sinh(g.|v_p|.t)$$

where$\hat{A}$ is a slowly varying complex amplitude of the mode and $|v_p|$ and $e^{i\vartheta}$ describe the pump field amplitude $v_p = |v_p|e^{i\vartheta}$. We can use these results to calculate the generated photon statistics.

However, the actual field generated is in fact polychromaticand multimode; we can thus describe it as a superposition of modes. Whenmodes are generated in a nonlinear block of crystal of volume $V = L^3$, the interactional Hamiltonian takes the form:

$$H_I = \frac{1}{2}\int_V \chi_{ijk}^{(2)} E_i(\vec{r},t)E_j(\vec{r},t)E_k(\vec{r},t)dV.$$

If we consider the frequency dependence of $\chi^{(2)}$, express *H* by means of Fourier components of $\vec{E}$ and quantize the field, we will finally get for the total energy the operator [3, 15]

$$\widehat{H_I} = \sum_{\vec{k},s} \hbar\omega(\vec{k})\hat{a}_{\vec{k},s}\hat{a}_{\vec{k},s}^{\dagger} + \frac{1}{L^3}\int_V \sum_{\vec{k}_1,s_1}\sum_{\vec{k}_2,s_2}\sum_{i,j,l=1}^{3} \chi_{ijl}^{(2)}(\vec{r};\omega(\vec{k}_p),\omega(\vec{k}_1),\omega(\vec{k}_2)).\hat{a}_{\vec{k}_1,s_1}^{\dagger}\hat{a}_{\vec{k}_2,s_2}^{\dagger}.$$

$$\times v_l.\left(\vec{\varepsilon}_{\vec{k}_1,s_1}^{*}\right)_i\left(\vec{\varepsilon}_{\vec{k}_2,s_2}^{*}\right)_j.e^{i((\vec{k}_p-\vec{k}_1-\vec{k}_2).\vec{r})}.e^{-i\left(\omega(\vec{k}_p)-\omega(\vec{k}_1)-\omega(\vec{k}_2)\right)t}$$

where $\vec{\varepsilon}_{\vec{k},s}$ is a unit polarization vector with dependence on $\vec{k}$ and polarization index *s*=1,2 and v_l are pump amplitude vector components. In the interaction picture, the dependence of the field state on time is given by [3, 14]:

$$|\psi(t)\rangle = \hat{T} exp\left[\frac{1}{i\hbar}\int_0^t \hat{H}_I(t')\,dt'\right]|\psi(0)\rangle.^{1}$$

If we do the calculation, suppose that the generated modes are initially in the vacuum and take into account post-selection according to the phase matching conditions (signal and idler photons are carefully selected by apertures and have similar polarizations, so only sum over the frequencies is considered), we get the expression

$$|\psi(t)\rangle = m|vac\rangle_1|vac\rangle_2 + \frac{\eta v \delta\omega}{2\pi}\sum_{\omega_1}\sum_{\omega_2}\phi(\omega_1,\omega_2)\frac{sin\left[\frac{1}{2}(\omega_1+\omega_2-\omega_p)t\right]}{\frac{1}{2}(\omega_1+\omega_2-\omega_p)}$$

$$\times exp\left[\frac{-i(\omega_p-\omega_1-\omega_2)t}{2}\right].\hat{a}^\dagger_{\omega_1}\hat{a}^\dagger_{\omega_2}|vac\rangle_1|vac\rangle_2 + higher\ order\ terms \qquad (2.3)$$

where m and η are constants, $\delta\omega$ is the modes spacing and the spectral function $\phi(\omega_1,\omega_2)$ determines the frequency dependencies of χ. If we then take ϕ to be normalized, that is,

$$\left(\frac{1}{2\pi}\right)\int_0^\infty \left|\phi(\omega,\omega_p-\omega)\right|^2 d\omega = 1,$$

and allow for the normalization of$|\psi(t)\rangle$,$\langle\psi(t)|\psi(t)\rangle = 1$ and consider a long *t* we obtain the condition

$$|m|^2 + |\eta v|^2 t = 1.$$

Therefore the approximation above only holds if $|\eta v|^2 t \ll 1$ as the constant $|m|$ is close to 1 (photon pairs are rarely emitted). This means that *t* has to be sufficiently short with respect to the average time between two down-conversion processes [14]. The higher order terms in expression (2.3) can be safely omitted in the case of short-term pumping; in the case of continuous pumping, the term $|\eta v|^2$ then functions as the probability of photon pair generation per unit time [3].

2.2.3 Detection Rates

The down-conversion rate can be calculated as

[1] $\hat{T}$ is the time-ordering operator.

$$R(t) = \alpha\langle\psi(t)|\hat{E}^{(-)}(t)\hat{E}^{(+)}(t)|\psi(t)\rangle \qquad (2.4)$$

where we have counted in the detection efficiency α, here assumed to be frequency-independent, and $\hat{E}^{(+)}(t)$ and $\hat{E}^{(-)}(t)$ represent positive and negative-frequency parts of the field operator $\hat{E} = \hat{E}^{(+)}(t) + \hat{E}^{(-)}(t)$,

$$\hat{E}^{(+)}(t) = \left[\hat{E}^{(-)}(t)\right]^{\dagger} = \sqrt{\frac{\delta\omega}{2\pi}}\sum_{\omega}\hat{a}_{\omega}e^{-i\omega(t-\Delta t)}, \qquad (2.5)$$

$c\Delta t$ being the distance of the detector from the crystal along the beam. Performing the calculation (2.4), we will finally obtain

$R_s(t) = \alpha_s|\eta v|^2$ and $R_i(t) = \alpha_i|\eta v|^2$ for signal and idler photons [3, 14].

However, in our experiment, we are mainly interested in the coincidence rate that gives the number of coincident detections at two detectors D1 and D2 placed in the signal and idler paths respectively; or, more generally, the rate of detections displaced by a predefined time interval τ:

$$R_{12}(t, t+\tau) = \alpha_1\alpha_2\langle\psi(t)|\hat{E}_1^{(-)}(t)\hat{E}_2^{(-)}(t+\tau)\hat{E}_2^{(+)}(t+\tau)\hat{E}_1^{(+)}(t)|\psi(t)\rangle. \qquad (2.6)$$

2.2.4 General Description of the Output State

The field obtained by post-selection of two directions satisfying the phase matching conditions after the crystal and limiting the spatial and polarization modes of photon pairs can in general be approximated by:

$$|\psi\rangle = \int_{\omega}\phi(\omega, \omega_p - \omega)\,|\omega\rangle_i\big|\omega_p - \omega\big\rangle_s d\omega, \qquad (2.7)$$

as a finite pass band nevertheless allows a spectrum of finite width;$|\omega\rangle$ is the state of a single photon in the idler (*i*) or signal (*s*) modes and ϕ is the spectral function describing the presence of individual frequencies– it is determined predominantly by the spectral filter we use to post-select down-converted pairs [15].

2.3 Beam Splitter

2.3.1 Quantum-mechanical description

In the quantum-mechanical description of a beam splitter, we have to take into account two input and two output ports: whereas in the classical case, the unused input port makes no

difference in the calculation as it does not contain a mode, in the quantum picture the vacuum still contains a mode.

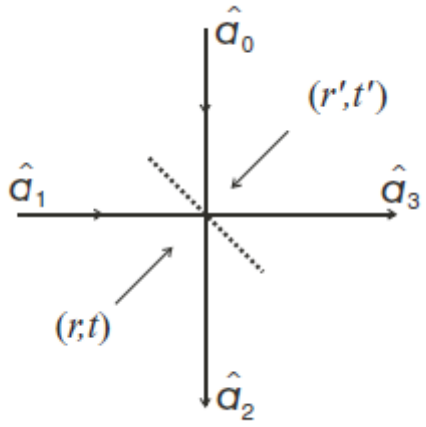

Fig. 2.5: Quantum-mechanical picture of a beam splitter. Source: 10.

In analogy to the classical case, we can describe the beam splitter by means of its reflectances and transmittances *r, r'* and *t, t'* corresponding to the two input ports and the input and output modes by means of annihilation operators (see Fig. 2.5 above):

$\hat{a}_2 = r\hat{a}_1 + t'\hat{a}_0$

$\hat{a}_3 = t\hat{a}_1 + r'\hat{a}_0$, or,

$$\begin{pmatrix}\hat{a}_2\\ \hat{a}_3\end{pmatrix} = \begin{pmatrix}r & t'\\ t & r'\end{pmatrix}\begin{pmatrix}\hat{a}_1\\ \hat{a}_0\end{pmatrix} \qquad (2.8)$$

The following commutation relations for creation and annihilation operators, valid for bosons, have to be satisfied:

$\left[\hat{a}_i, \hat{a}_j^\dagger\right] = \delta_{ij}$ and $\left[\hat{a}_i, \hat{a}_j\right] = \left[\hat{a}_i^\dagger, \hat{a}_j^\dagger\right] = 0.$

It can be shown that the following conditions, known as reciprocity conditions, hold:

$|r'| = |r|, |t'| = |t|, |r|^2 + |t|^2 = 1, r^*t' + r't'^* = 0$ and $r^*t + r't'^* = 0.$

The phase shift induced by the beam splitter depends on its coating design [16]. For a 50:50 beam splitter with a single dielectric layer, we get:

$\hat{a}_2 = \frac{1}{\sqrt{2}}(\hat{a}_0 + i\hat{a}_1)$ and $\hat{a}_3 = \frac{1}{\sqrt{2}}(\hat{a}_1 + i\hat{a}_0),$ (2.9)

the reflected beams shifted in phase by $\frac{\pi}{2}$ with respect to the transmitted ones.

We may also express the action of a beam splitter in the Heisenberg picture by means of a unitary transformation:

$$\begin{pmatrix}\hat{a}_2\\ \hat{a}_3\end{pmatrix} = \hat{U}^{\dagger}\begin{pmatrix}\hat{a}_1\\ \hat{a}_0\end{pmatrix}\hat{U}$$

where $\hat{U}$ is a unitary operator which in case of a 50:50 beam splitter takes the form $\hat{U} = e^{i\frac{\pi}{4}\hat{A}}$ with $\hat{A} = \hat{a}_0^{\dagger}\hat{a}_1 + \hat{a}_0\hat{a}_1^{\dagger}$.

2.3.2 Single-Photon Incidence

However, we are more interested in output states that can be constructed using the relations (2.8). For example, if we consider a single photon incident on the 50:50 beam splitter described by (2.9) through port no. 1, we may write the input state as:

$$|0\rangle_0|1\rangle_1 = \hat{a}_1^{\dagger}|0\rangle_0|0\rangle_1.$$

From (2.9), we find that

$$\hat{a}_1 = \frac{1}{\sqrt{2}}(\hat{a}_3 - i\hat{a}_2)$$

and therefore, $\hat{a}_1^{\dagger} = \frac{1}{\sqrt{2}}\left(\hat{a}_3^{\dagger} + i\hat{a}_2^{\dagger}\right)$. (2.10)

Hence, we may write the output state:

$$\hat{a}_1^{\dagger}|0\rangle_0|0\rangle_1 \rightarrow \frac{1}{\sqrt{2}}\left(\hat{a}_3^{\dagger} + i\hat{a}_2^{\dagger}\right)|0\rangle_2|0\rangle_3 = \frac{1}{\sqrt{2}}\left(i|1\rangle_2|0\rangle_3 + |0\rangle_2|1\rangle_3\right),$$

$$|\psi_{out}\rangle = \frac{1}{\sqrt{2}}\left(i|1\rangle_2|0\rangle_3 + |0\rangle_2|1\rangle_3\right). \quad (2.11)$$

We can see that the result is a superposition of the output photon being reflected and transmitted and no coincidence counts can be expected from the detectors placed at the outputs 2 and 3. Yet if a Mach-Zehnder interferometer is constructed using two beam splitters, that is, outputs 2 and 3 are again combined at another beam splitter, interference between the two path alternatives can be observed (see 2.3.4 below). Such single-photon

interference was a key element in our experimental setup as described in more detail in the next chapter.

2.3.3 Two-Photon Incidence

However, an important case for our experiment is that of two single photons arriving at the 50:50 beam splitter simultaneously by the two input ports. The input state is now therefore:

$|1\rangle_0|1\rangle_1 = \hat{a}_0^\dagger \hat{a}_1^\dagger |0\rangle_0|0\rangle_1$, $\hat{a}_1^\dagger$ is given by (2.9) and we find $\hat{a}_0^\dagger$ analogously from (2.8) to be equal to:

$$\hat{a}_0^\dagger = \frac{1}{\sqrt{2}}\left(\hat{a}_2^\dagger + i\hat{a}_3^\dagger\right). \qquad (2.12)$$

Hence

$$\hat{a}_0^\dagger \hat{a}_1^\dagger |0\rangle_0|0\rangle_1 \rightarrow \frac{1}{2}\left(\hat{a}_2^\dagger + i\hat{a}_3^\dagger\right)\left(\hat{a}_3^\dagger + i\hat{a}_2^\dagger\right)|0\rangle_2|0\rangle_3 = \frac{i}{2}\left(\hat{a}_2^\dagger \hat{a}_2^\dagger + \hat{a}_3^\dagger \hat{a}_3^\dagger\right)|0\rangle_2|0\rangle_3$$

$$|\psi_{out}\rangle = \frac{i}{\sqrt{2}}|2\rangle_2|0\rangle_3 + |0\rangle_2|2\rangle_3 \qquad (2.13)$$

as $\hat{a}^\dagger|n\rangle = \sqrt{n+1}|n+1\rangle$. Two photons arriving at the beam splitter each in one of the input ports thus always exit the beam splitter together; they are either both transmitted or both reflected. The same result can be obtained if we think of the problem in terms of probability amplitudes of the possible results: if we then calculate the probability of a photon exiting the 50:50 beam splitter in each of the output ports, we will get 0 [10]. However, we have to bear in mind that this reasoning is simplified for idealized monochromatic photons and a 50:50 beam splitter. The effect was first experimentally demonstrated by Hong, Ou and Mandel [16] when they used it to measure the time interval between a pair of down-converted photons. It is also fundamental to our experimental setup (see the following chapter) and described in more detail below.

2.4 Mach-Zehnder Interferometer

The Mach-Zehnder (MZ) interferometer is one of the elementary interferometric setups particularly useful for observing single photon interference. Its basic structure contains two 50:50 beam splitters, two mirrors and two detectors. The path length difference between the two interferometer arms can be adjusted by placing a phase shifter in one of them (see

Fig. 2.6). Light enters the interferometer through the first beam splitter and is combined at the second; if the two optical paths are balanced (with respect to the coherence properties of the light source), we can observe interference at detectors D1 and D2 depending on the relative phase shift between the two arms θ. The intensities on the two detectors depend on the incoming intensities, relative phase shift and complex degree of coherence (number the absolute value of which describes the amount of coherence between the two incoming amplitudes) in the following manner [6]:

$$I_{D1} = I_1 + I_2 + 2\sqrt{I_1 I_2}.cos\theta|\gamma_{12}(\tau)|$$

$$I_{D2} = I_1 + I_2 + 2\sqrt{I_1 I_2}.sin\theta|\gamma_{12}(\tau)|.$$

The intensity of the interference effect is described by visibility (2.14):

$$V = \frac{I_{MAX} - I_{MIN}}{I_{MAX} + I_{MIN}} = 2.\frac{\sqrt{I_1 I_2}}{I_1 + I_2}|\gamma_{12}(\tau)|$$

thus if $I_1 = I_2$ we get $V = |\gamma_{12}(\tau)|$ – visibility is equal to the absolute value of the degree of coherence.[2]

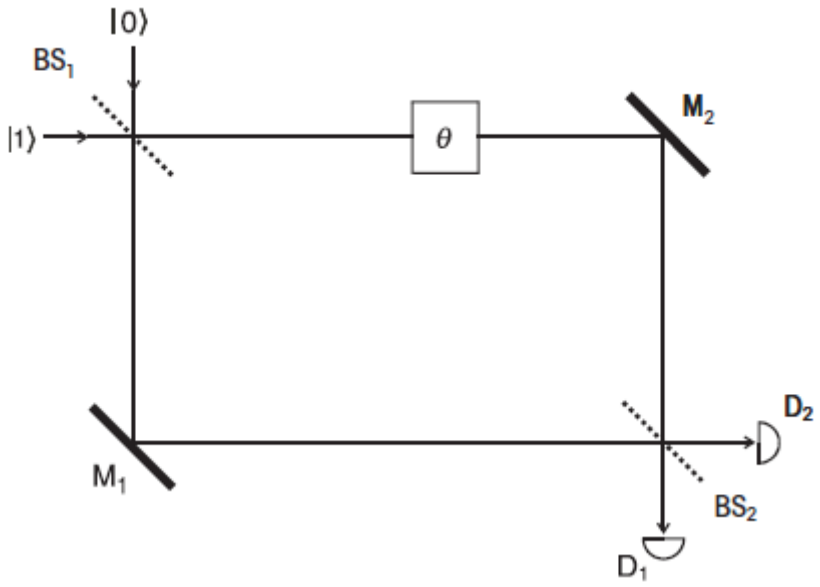

Fig. 2.6: The Mach-Zehnder interferometer. BS1, BS2 – beam splitters, M1,M2 – mirrors, D1, D2 – detectors, θ - phase shifter. Source: [10].

[2] In reality, visibility is influenced by several other factors such as e.g. the distinguishability of polarization states. This will be made clear in the description of the experiment.

Now if we consider a single photon entering the apparatus, with the beam splitters described by (2.9), its state gets transformed at BS1 in the following way (see Eq. 2.11) – the mirrors contribute to each of the resulting possible states with a phase factor of $e^{i\frac{\pi}{2}}$equally so their contribution can be omitted:

$|0\rangle|1\rangle \xrightarrow{BS1} \frac{1}{\sqrt{2}}(i|1\rangle|0\rangle + |0\rangle|1\rangle).$

However, the phase shifter produces a relevant phase shift in the upper interferometer arm, thus transforming the state as follows:

$\frac{1}{\sqrt{2}}(i|1\rangle|0\rangle + |0\rangle|1\rangle) \xrightarrow{\theta} \frac{1}{\sqrt{2}}\left(i|1\rangle|0\rangle + e^{i\theta}|0\rangle|1\rangle\right).$

The second beam splitter transforms individual terms of the resulting state:

$|0\rangle|1\rangle \xrightarrow{BS2} \frac{1}{\sqrt{2}}(i|1\rangle|0\rangle + |0\rangle|1\rangle)$

$|1\rangle|0\rangle \xrightarrow{BS2} \frac{1}{\sqrt{2}}(|1\rangle|0\rangle + i|0\rangle|1\rangle)$, and the total transformation can be written:

$$\frac{1}{\sqrt{2}}\left(i|1\rangle|0\rangle + e^{i\theta}|0\rangle|1\rangle\right) \xrightarrow{BS2} \frac{1}{2}\left(e^{i\frac{\pi}{2}}|1\rangle|0\rangle - |0\rangle|1\rangle + e^{i\left(\theta+\frac{\pi}{2}\right)}|1\rangle|0\rangle + e^{i\theta}|0\rangle|1\rangle\right) =$$

$$= \frac{1}{2}\left[\left(e^{i\theta}-1\right)|0\rangle|1\rangle + \left(\left(e^{i\theta}+1\right)i|1\rangle|0\rangle\right)\right]$$

Thus the probability of obtaining the state $|0\rangle|1\rangle$, that is detector D2 firing, is

$$P_{|0\rangle|1\rangle} = \left|\frac{e^{i\theta}-1}{2}\right|^2 = \left(\frac{cos\theta - 1}{2}\right)^2 + \left(\frac{sin\theta}{2}\right)^2 = \frac{1}{2}(1 - cos\theta)$$

and the probability of obtaining the state$|1\rangle|0\rangle$, that is detector D1 firing, is

$$P_{|1\rangle|0\rangle} = \left|i\frac{e^{i\theta}+1}{2}\right|^2 = \left(\frac{cos\theta + 1}{2}\right)^2 + \left(\frac{sin\theta}{2}\right)^2 = \frac{1}{2}(1 + cos\theta).$$

Consequently, we can observe interference fringes of sinusoidal character when θ is varied (see Fig.2.7 below).

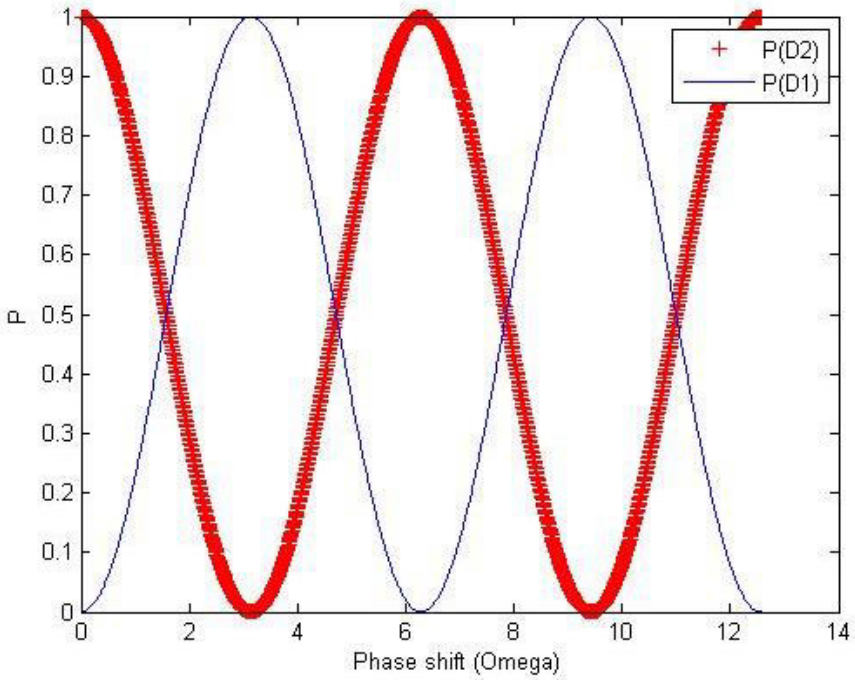

Fig. 2.7: Probabilities of detecting a photon produce interference fringes at detectors D1 and D2

2.5 Hong-Ou-Mandel Effect

As it was explained in 2.3.3, when two identical photons arrive at a 50:50 beam splitter, each in one of the input ports, they always exit the beam splitter in one of the output ports together and if these contain detectors, no coincidence counts are measured between them (see relation (2.13)). This effect was experimentally shown for the first time by Hong, Ou and Mandel [17] and has been since commonly referred to as the HOM effect. In their experiment, Hong, Ou and Mandel initially used it to measure the time displacement of two identical photons generated by SPDC; now it represents a fundamental way of measuring the overlap of two photons. The original experimental setup is depicted in Figure 2.8 below.

Photon pairs were generated in a parametric down-convertor, post-selected by a filter and subsequently recombined at a beam splitter. Two detectors were placed at the outputs of the beam splitter mounted on a translation stage so that the difference between their optical paths could be varied and coincident counts from detectors D1 and D2 were measured. The interference filters placed after the pinholes determined the photons time coherence interval to be of the order of 10^{-13} s. It was thus possible to obtain the interference effect expressed by (2.13) above if the idler and signal states overlapped within this time interval.

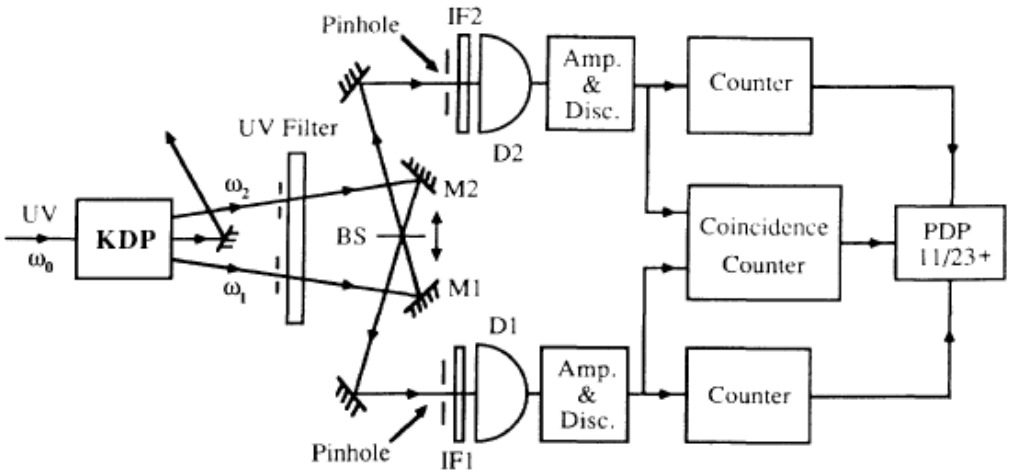

Fig. 2.8: Original setup of the Hong-Ou-Mandel experiment. Source: [17].

In Section 2.3.3 of this chapter, we considered a 50:50 splitting ratio of the beam splitter for simplicity; the more general case for a monochromatic approximation of the output state would be [17] (the reflected photons acquire a phase shift of $e^{i\frac{\pi}{2}} = i$):

$$|\psi_{out}\rangle = (R-T)|1\rangle_2|1\rangle_3 + i\sqrt{2RT}|2\rangle_2|0\rangle_3 + i\sqrt{2RT}|0\rangle_2|2\rangle_3, \quad (2.13)$$

where *R* and *T* stand for reflectivity and transmissivity of the beam splitter respectively which are $R = |A_R|^2$ and $T = |A_T|^2$, that is square moduli of the probability amplitudes for reflection and transmission. Furthermore, it also has to be taken into account that the state of the down-converted photons selected by the pinholes and interference filters is not perfectly monochromatic and should rather be expressed as a superposition of frequency contributions in a certain frequency range, as given by (2.76). From these considerations, Hong, Ou and Mandel calculated the probability of coincident detections and consequently the coincidence rate N_c, showing its dependence on the time displacement of the photons δt given by the actual beam splitter displacement $d = c\delta t$ [17]:

$$N_c = C(T^2 + R^2)\left[1 - \frac{2RT}{T^2+R^2}e^{-(\Delta\omega\delta t)^2}\right]. \quad (2.15)$$

where*C* is a constant and $\Delta\omega$ the pass band of the interference filters. Thus in the ideal case of *R*=*T*, we would then get:

$$N_c = K\left[1 - e^{-\left(\frac{\Delta\omega d}{c}\right)^2}\right].$$

This exponential dependence of coincidence rate on the path difference has the form of a dip centred at $\delta t = 0$ as verifiedby the HOM experiment (see Fig. 2.9 below).

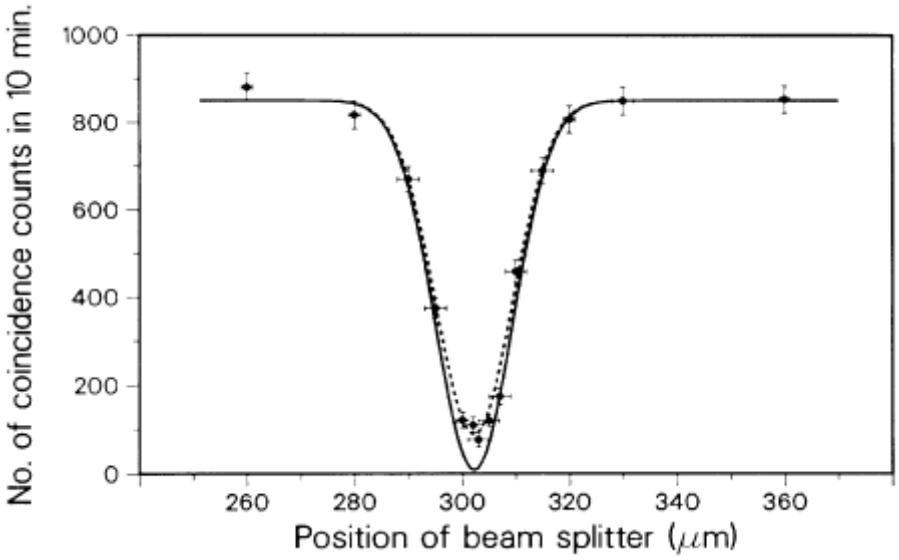

Fig. 2.9: Experimental result of the Hong, Ou and Mandel's experiment – the so-called HOM dip. Source : [17].

In our experiment, we used an HOM-type setup to characterize our source and target qubits and measure the parameter *D* see (Section 2.1 above).

2.6 Direct Measurement of Indistinguishability

$|D|$ can be measured experimentally using two photonic qubits and a setup based on the HOM effect, that is, by means of a beam splitter and coincidence detection, and varied by varying the delay between the two photons. A good source of photon pairs suitable for carrying the qubits is SPDC; if we take into account the possible delay between them, their state can be expressed as, in accordance with relation (2.7)

$$|\psi\rangle = \int_{\omega} \phi(\omega)\phi(\omega_p - \omega)\, e^{-i\omega\Delta t} |\omega\rangle_a \big|\omega_p - \omega\big\rangle_b d\omega, \qquad (2.16)$$

where the state $|\omega\rangle_a$ represents a single photon in the spatial mode *a* and ϕ is a spectral amplitude function that can primarily be shaped by the interference filter used when building the source. A 50:50 beam splitter performs a unitary transformation on the input states $|\psi\rangle$ in the following way:

$$|\varphi\rangle = U_{BS}|\psi\rangle$$

where the creation operators of input modes are related to those of output modes by the creation/annihilation operator relations according to (2.10) and (2.12) with $a = a_0, b = a_1, c = a_2$ and $d = a_3$. The resulting coincidence rate can be calculated (see 2.4) as proportional to:

$$R(\Delta t) \propto \int_{t_1} \int_{t_2} \langle \varphi | E_c^{(-)}(t_1) E_d^{(-)}(t_2) E_d^{(+)}(t_2) E_c^{(+)}(t_1) | \varphi \rangle$$

with positive and negative-frequency parts of an electric field operator given by (2.5).

It is possible to show that [1]:

$$R(\Delta t) \propto 1 - \mathrm{Tr}[F|\psi\rangle\langle\psi|] = 1 - D \qquad (2.17)$$

where the flip operator $F = \int_{\omega_1} \int_{\omega_2} |\omega_1\rangle_c |\omega_2\rangle_d \langle\omega_2|_c \langle\omega_1|_d$. For the state (2.16) above, D can be found proportional to:

$$D \propto \int_{\omega} \left|\phi\left(\frac{\omega_0 + \omega}{2}\right)\right|^2 \left|\phi\left(\frac{\omega_0 - \omega}{2}\right)\right|^2 e^{i\omega\Delta t}.$$

For a rectangular ϕ of spectral width v and central frequency ω_0, we thus get $D = \mathrm{sinc}(\Delta t v)$ and the HOM dip correspondingly has the shape of a reversed sinc function (compare with experimental data and Figures 3.9 or 4.1).

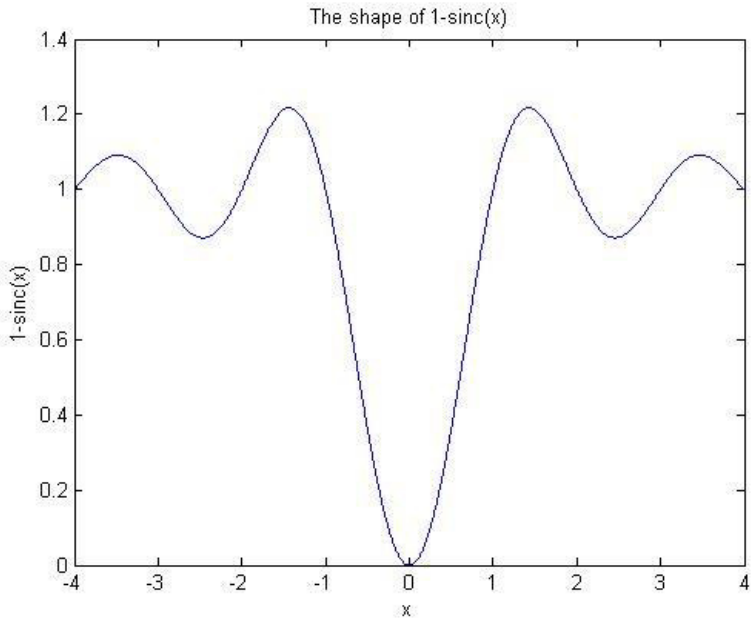

Fig. 2.10: According to the theory, the shape of the dependence of coincidence rate $R(\Delta t)$ [counts per unit time] on Δt [ps] for a rectangular spectral function agrees with that of 1-sinc(x).

3 Experiment

3.1 Underlying Principle

3.1.1 Qubit State Transfer

We have demonstrated the meaning the parameter *D* (see Eq. (2.1)) quantifying effective indistinguishability might have in quantum information protocols in an experiment where a transfer of a quantum state from one qubit to another was implemented without direct interaction. As no other resources were required in this transfer, its quality was influenced by indistinguishability alone and the fidelity of the states transferred was directly proportional to$|D|$. In our transfer protocol, we used two photonic qubits in dual-rail representation, one of which we will refer to as source (*S*) and the other as target (*T*).

3.1.2 Initial state

The state of the *S* qubit was prepared so that:

$$|\Psi\rangle_S = \frac{1}{\sqrt{2}}\left(|0,1\rangle_S + e^{i\theta}|1,0\rangle_S\right) \qquad (3.1)$$

where we have chosen for clarity the more compact notation $|0,1\rangle$ to denote the state $|0\rangle|1\rangle$, that is, the photon present in the "second" rail and $|1,0\rangle$ for $|1\rangle|0\rangle$, that is, the photon present in the "first" rail; the order of the rails being of course arbitrary. In our experiment, the phase θ was preset, but could in principle be unknown. The state of qubit *S* was to be transferred to qubit *T* which was initially in the state:

$$|\Phi\rangle_T = \frac{1}{\sqrt{2}}\left(|0,1\rangle_T + |1,0\rangle_T\right). \qquad (3.2)$$

We considered the effective distinguishability of the two photons dependent only on their degrees of freedom other than the optical path modes. In other words, all their physical differences were supposed to be contained in the state of their internal environment that can be represent by the density matrix

$$\rho_{E,ST} = \sum_{i,j,k,l} c_{i,j,k,l}|\psi_i\rangle_{E,S}\langle\psi_j| \otimes |\psi_k\rangle_{E,T}\langle\psi_l| \qquad (3.3)$$

where we sum over all basis states $|\psi_k\rangle$ of all environmental degrees of freedom of the two qubits. Therefore, the total state entering our transfer protocol was

$$\rho_{ini} = |\Psi\rangle_S\langle\Psi| \otimes |\Phi\rangle_T\langle\Phi| \otimes \rho_{E,ST}. \qquad (3.4)$$

3.1.3 Final state

Out of the four combinations of possible basis states of the whole system $|0,1\rangle_S|1,0\rangle_T|\psi_i\rangle_{E,S}|\psi_k\rangle_{E,T}$, $|1,0\rangle_S|0,1\rangle_T|\psi_i\rangle_{E,S}|\psi_k\rangle_{E,T}$, $|0,1\rangle_S|0,1\rangle_T|\psi_i\rangle_{E,S}|\psi_k\rangle_{E,T}$ and $|1,0\rangle_S|1,0\rangle_T|\psi_i\rangle_{E,S}|\psi_k\rangle_{E,T}$ we only kept the first two by post-selecting them via coincidence measurement: the latter two where two photons were present at one output were excluded.

The transfer was performed by swapping two rails between the qubits and subsequent measurement on *S*. The system thus first underwent the change

$|0,1\rangle_S|1,0\rangle_T|\psi_i\rangle_{E,S}|\psi_k\rangle_{E,T} \longrightarrow |0,1\rangle_S|1,0\rangle_T|\psi_k\rangle_{E,S}|\psi_i\rangle_{E,T}$ (environmental basis states swapped)

$|1,0\rangle_S|0,1\rangle_T|\psi_i\rangle_{E,S}|\psi_k\rangle_{E,T} \longrightarrow |1,0\rangle_S|0,1\rangle_T|\psi_i\rangle_{E,S}|\psi_k\rangle_{E,T}$ (no change)

which yielded the state

$$\rho_{trans} = \sum_{i,j,k,l} c_{i,j,k,l}\left|\Psi_{i,k}\right\rangle\left\langle\Psi_{j,l}\right|$$

with $|\Psi_{i,k}\rangle = \frac{1}{\sqrt{2}}\left[|1,0\rangle_S|0,1\rangle_T|\psi_i\rangle_{E,S}|\psi_k\rangle_{E,T} + e^{i\theta}|0,1\rangle_S|1,0\rangle_T|\psi_k\rangle_{E,S}|\psi_i\rangle_{E,T}\right]$.

When we trace out the environment,

$\rho_{ST} = \sum_{i,j}\langle\psi_i|_{E,S}\langle\psi_j|_{E,T}\,\rho_{trans}|\psi_i\rangle_{E,S}|\psi_j\rangle_{E,T}$,

we get the partially entangled state

$$\rho_{ST} = \frac{1}{2}\{|1,0\rangle_S\langle 1,0| \otimes |0,1\rangle_T\langle 0,1| + |0,1\rangle_S\langle 0,1| \otimes |1,0\rangle_T\langle 1,0| + \left[De^{i\theta}|0,1\rangle_S\langle 1,0| \otimes |1,0\rangle_T\langle 0,1| + De^{-i\theta}|1,0\rangle_S\langle 0,1| \otimes |0,1\rangle_T\langle 1,0|\right]\},$$

where D corresponds to the flipping of environmental basis states:

$$D = \sum_{i,j} c_{ij,ji} = Tr[F\rho_{E,ST}].$$

A projective measurement

$\Pi_{S,\pm} = |\pm\rangle_S\langle\pm|$, where $|\pm\rangle_S = \frac{1}{\sqrt{2}}\left(|0,1\rangle_S \pm |1,0\rangle_S\right)$

was performed on qubit S which transferred the original state of *S* onto *T*, so that, according to the measurement result $|\pm\rangle$:

$$\rho_T^{\pm} = \frac{1}{4}\left(\langle 0,1|_S \pm \langle 1,0|_S\right)\rho_{ST}\left(|0,1\rangle_S \pm |1,0\rangle_S\right)$$

$$= \frac{1}{4}\left\{|0,1\rangle_T\langle 0,1| + |1,0\rangle_T\langle 1,0| \pm De^{i\theta}|0,1\rangle_T\langle 1,0| \pm De^{-i\theta}|1,0\rangle_T\langle 0,1|\right\}.$$

If the measurement result was $|-\rangle$, we applied a corrective phase shift of π[3] onto the optical mode $|1,0\rangle_T$,such that

$|1,0\rangle_T \xrightarrow{\pi\ shift} e^{i\pi}|1,0\rangle_T = -|1,0\rangle_T$, so that we got the same state for $|+\rangle$ and for $|-\rangle$:

$$|+\rangle \xrightarrow{\pi} \rho_T = \frac{1}{4}\left\{|0,1\rangle_T\langle 0,1| + |1,0\rangle_T\langle 1,0| + De^{i\theta}|0,1\rangle_T\langle 1,0| + De^{-i\theta}|1,0\rangle_T\langle 0,1|\right\}$$

$$\left|-\right\rangle \xrightarrow{\pi} \rho_T = \frac{1}{4}\left\{|0,1\rangle_T\langle 0,1| - |1,0\rangle_T(-1)\langle 1,0| - De^{i\theta}|0,1\rangle_T(-1)\langle 1,0| + De^{-i\theta}|1,0\rangle_T\langle 0,1|\right\}$$

$$= \frac{1}{4}\left\{|0,1\rangle_T\langle 0,1| + |1,0\rangle_T\langle 1,0| + De^{i\theta}|0,1\rangle_T\langle 1,0| + De^{-i\theta}|1,0\rangle_T\langle 0,1|\right\}.$$

The final state could thus be written

$$\rho_{fin} = \frac{1}{2}\left\{|0,1\rangle_T\langle 0,1| + |1,0\rangle_T\langle 1,0| + De^{i\theta}|0,1\rangle_T\langle 1,0| + De^{-i\theta}|1,0\rangle_T\langle 0,1|\right\}$$

which expressed by means of the initial state of *S* gives

$$\boxed{\rho_{fin} = \frac{1+D}{2}|\Psi\rangle_S\langle\Psi| + \frac{1-D}{2}|\Psi^{\perp}\rangle_S\langle\Psi^{\perp}|,} \qquad (3.5)$$

where the orthogonal complement of $|\Psi\rangle_S$:

$|\Psi^{\perp}\rangle_S = \frac{1}{\sqrt{2}}\left(|0,1\rangle_S - e^{i\theta}|1,0\rangle_S\right)$.

[3] See Section 3.2.1.9 for information on physical implementation.

The expression (3.5) can be interpreted as the original state of S modified by decoherence which is quantified by a factor involving *D*. The sign of *D* does not have a major significance; if it is known before the experiment, it can be compensated by the application of another conditional phase shift. $|D|$ therefore determines the quality of quantum state transfer, but it should be noted that perfect transfer $|D| = 1$ can correspond to three different states $\rho_{E,ST}$:

- product of pure perfectly overlapping single-particle states: $D = 1$
- symmetric maximally entangled states: $D = 1$
- antisymmetric maximally entangled states: $D = -1$

This also means that if $|D| = 1$, entangled particles behave as if they were in a factorable state. However, *D* would vary in a different way in each of these cases under the application of local unitary operators $U_{ES} \otimes V_{ET}$ where U_{ES} differs from V_{ET}.

3.2 Experimental Setup

3.2.1 General Description

To implement the transfer protocol, we have advantageously employed a fibre-optical setup we were well familiar with and which served previously as the basis of a fibre-optical programmable phase gate operating with 50% success probability [6, 18].

The source and target qubits were carried by two down-converted photons fed into two fibre couplers whose two output optical modes then created the qubit basis states $|0\rangle$ and $|1\rangle$. With regard to the theoretical viewpoint discussed above, we preferred the notation $|0,1\rangle$ and $|1,0\rangle$, the first state being that of a photon present in an outer rail, the latter that of a photon present in an inner rail (see Fig. 3.1 below). Although we have seen the phase factor in *S* appears with the basis state $|1,0\rangle_S$, it was in fact set by the phase modulator PM_{st}. We nevertheless obtained state (3.1) by applying a negative phase shift of $-\theta$ in the upper rail of the source qubit interferometer, as a phase shift of θ in one arm of the interferometer is physically equivalent to a phase shift of $-\theta$ in the other (the overall phase is physically insignificant):

$$|\Psi\rangle_S = \frac{1}{\sqrt{2}}\left(|0,1\rangle_S + e^{i\theta}|1,0\rangle_S\right) = \frac{1}{\sqrt{2}}e^{i\theta}\left(e^{i(-\theta)}|0,1\rangle_S + |1,0\rangle_S\right).$$

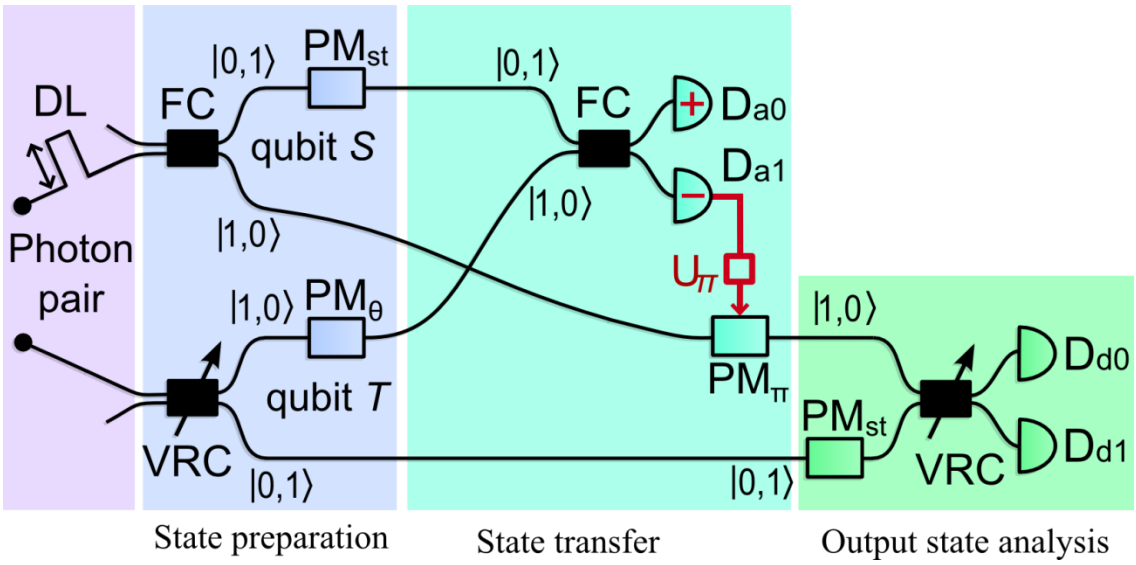

Fig. 3.1: Experimental setup. DL – delay line, FC – 50:50 fibre coupler, VRC – variable ratio couplers (the first variable ratio coupler was preset to 50:50), PM – phase modulators, D – detectors. Source: adapted from a version published in [1] and created by Martina Mikova.

The quantum state transfer from qubit *S* onto qubit *T* was realized by means of swapping two rails between the qubits: projective measurement on qubit S, realized by joining its two optical modes in a fibre coupler and placing two detectors at its outputs, transferred the phase present in *S* onto *T*. A measurement was carried out at the output of *T* in its turn and the total output state was reconstructed by means of quantum state tomography to evaluate the transfer performed. The two beam splitters and the optical modes between them thus formed two intertwined Mach-Zehnder interferometers. Only the cases when one photon was present in each interferometer were considered as we only kept record of coincident detections between the detectors at the outputs of *S* and *T*.

The detection of S corresponded to a projective measurement performed in the basis $|\pm\rangle_S = \frac{1}{\sqrt{2}}\left(|0,1\rangle_S \pm |1,0\rangle_S\right)$. Detector D_{a1} firing corresponded to $|-\rangle_S$ and a corrective phase shift was applied onto *T* to compensate for this phase difference of π by means of feed-forward (see below for more on the technique of feed forward).At the output of the setup, counts were collected by detectors D_{d0} and D_{d1}; qubit *T* was measured in three different bases set by means of a variable ratio coupler (VRC) and a phase modulator, so that we could have enough data to characterize its output state by subsequent quantum tomography.

As the setup consisted in principle of two fibre Mach-Zehnder interferometers, its design had to deal with two key issues: lengths of the arms had to be balanced and polarization states in both arms had to overlap to reach high visibilities and phase drift caused by various mechanical effects (air circulation, acoustic vibrations and fluctuations of temperature) had to be dealt with. The first prerequisite was accomplished via motorized air gaps in each of the arms in which polarizers and wave plates were placed to permit accurate setting of the polarization. The second issue was resolved by both passive and active stabilization; the passive method was provided by the vibration control of the optical table and isolation of the setup in a polystyrene box, the active one consisted in regular application of an automatic phase correcting procedure in between a few seconds long intervals, that is, between individual measurements, effectuated by means of phase modulators (PM_{st} – see Figure 3.1 above) placed in the arms of the interferometers. For the purpose of interferometers adjustment, the weak signal from the down-convertor would be inconvenient. For that reason, we adjusted the setup using a laser diode with a central wavelength corresponding to that of the down-converted photons.

Our measurement of indistinguishability also required us to be able to manipulate the overlap of the photon correlation times, in other words, to measure their HOM dip and adjust the photons to a certain delay corresponding to a point in the dip; to that end, a motorized stage was placed in the source to enable the changing of the photon arrival times in a controlled way.

3.2.2 Detailed Description

Before entering the core setup, photons generated by the source passed through linear fibre polarizers (P) with fixed axis; this ensured that they were fed into the setup with stable preset polarization that could then be adjusted in a controlled way to maximize the power transmitted through the setup and thus helped to maintain the output power. Transmission through the polarizers was optimized by means of polarization controllers (PC). Both input fibre couplers FC_{in} and VCR_{in} had a 50:50 splitting ratio (the former one having a fixed splitting ratio, the latter one being set to approximately 50:50, more precisely, 47:53, which nevertheless did not have significant influence on the quality of qubit transfer).

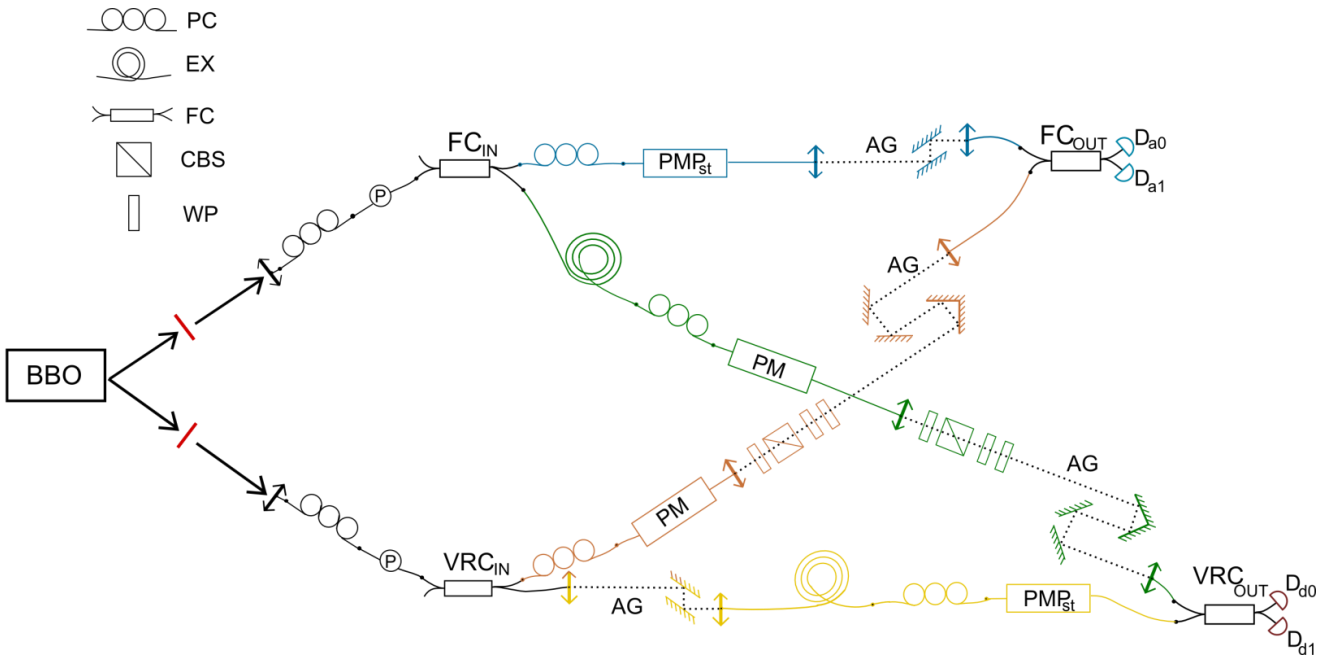

Fig. 3.2: Detailed experimental setup.[4] PC – polarization controller, EX – extra fibre, FC – fibre coupler (VRC – variable ratio coupler), CBS – cube beam splitter, WP – wave plate, P – polarizer, PM – phase modulator, PMP – phase modulator with an integrated polarizer, AG – air gap, D - detector.

The two intertwined interferometers had to be, each one in turn, optimized for transmission and visibility. Both interferometers incorporated an air gap of adjustable width that served for precision compensation of path length differences. The interferometer consisting of the $|1,0\rangle_S$ and $|0,1\rangle_T$ modes (in green and yellow in Fig. 3.3) contained additional fibre which provided sufficient delay necessary for the operation of feed-forward. Phase modulators present in all the rails had to be optimized for transmission via polarization controllers. Polarizing elements in the inner rails (in green and orange in Fig. 3.3) served to adjust the output polarization states as both path lengths and polarization states had to overlap well in order to reach high visibilities. The source qubit (blue and orange interferometer) was measured by means of a fixed ratio (50:50) output fibre coupler, whereas the coupler at the output of the longer (blue and yellow) interferometer had to have variable ratio so that we were able to change the measurement basis. Each of the detectors placed at the output of these fibre couplers were connected to coincident logic: coincidences between each pair of detectors were measured (6 coincidence channel altogether).

[4] See Part 5 Appendix for a full-sized scheme.

3.2.2.1 Source

The source consisting of a 405 nm blue laser diode, CUBE^{TM} by Coherent with 100 mW output power, a non-linear BBO (β-barium borate) crystal and an infrared 810 nm OZ optics laser diode with 1 mW power[5] and was built by Ivo Straka and Miroslav Ježek (for more information on the source, consult [9]). The blue laser served to pump the crystal to produce photon pairs, whereas the red one as probe for setup adjustment and later stabilization of the setup during measurement: the source was provided with computer operated choppers that would allow or block either beam when needed. Moreover, two electronic flippers were placed before the coupling lenses C1 and C2 (see Fig. 3.3), enabling us to block either beam or both. The red diode probe beam could conveniently be attenuated by means of an attenuator placed before the setup so that it could operate in both a strong regime, suitable for initial setup adjustment (see Section 3.2.3), and a weak regime from which the single photon detectors would not suffer damage, suitable for the stabilization of the setup (see Section 3.3.1.3).

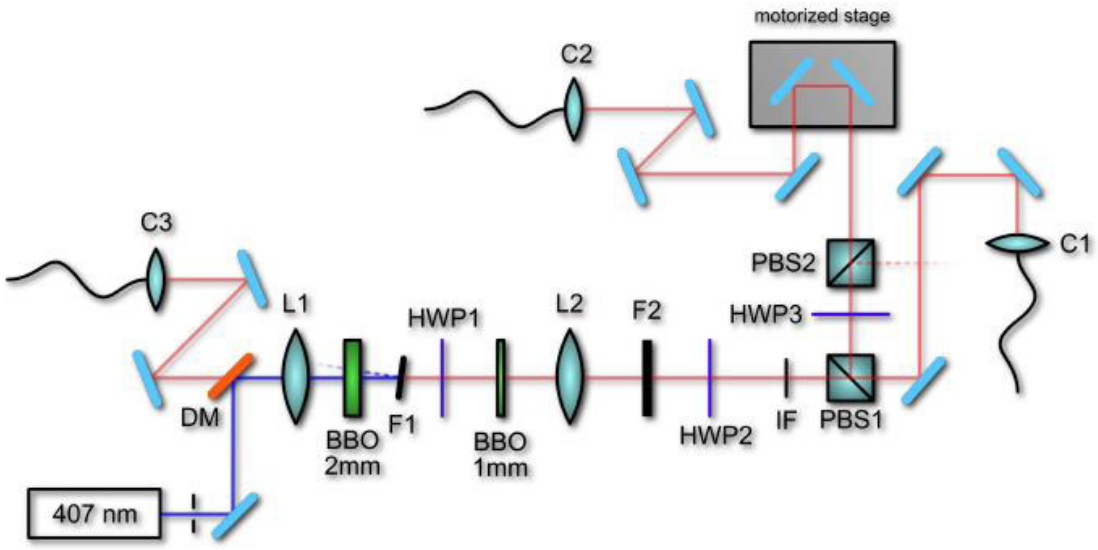

Fig. 3.3: Layout of the source setup. Source: created by Ivo Straka and published in [9]. DM – dichroic mirror (transmits red light, reflects blue light), L – lenses, HWP – half-wave plates, F – filters, IF – interference filter, PBS – polarization beam splitters, C – coupling lenses.

The non-linear crystal was prepared and installed in a way to enable degenerate type II collinear down-conversion. This means that the photon pairs that served as source and

[5] Auxiliary probe source for setup adjustment and stabilization.

target qubits in our experiment were generated in the same direction and with identical frequencies. The 405 nm pumping thus provided photons at around 810 nm; before entering the core setup, the photons passed by interference filters with approximately rectangular passband of 2.7nm FWHM centred at 810 nm. The narrow spectral width of the filter results in a relatively low output coincident rate, but also an improved visibility of the HOM dip for the two photons (around 99%, see section 3.9 in [9]). The HOM dip could be measured thanks to a motorized translation stage which provided a means of manipulating the difference between arrival times of the photons and therefore their time overlap.

3.2.2.2 Polarizers and Other Polarizing Elements

As mentioned in the introduction to this section, two fibre-optical linear polarizers were placed before the inputs of the setup to provide the setup with stable linear input polarization states. The polarizers were preceded by polarization controllers that gave us control over the polarization states entering them. We could thus easily optimize them for transmission and what is more, the combination of a polarization controller and a polarizer could be used for the reverse effect, that is to attenuate the signal when needed. Both polarizers were manufactured by OZ Optics (see [6] for details).

Furthermore, two bulk cube polarizing beam splitters were used together with other polarizing elements (half-wave plates and quarter-wave plates) in air gaps of the $|1,0\rangle$ modes (green and orange in Fig. 3.2 above). Polarizing beam splitters contain a diagonally placed internal face with a coating that divides incoming light into polarization components parallel (p) and perpendicular (s) to the plane of incidence (see Fig. 3.4 below).

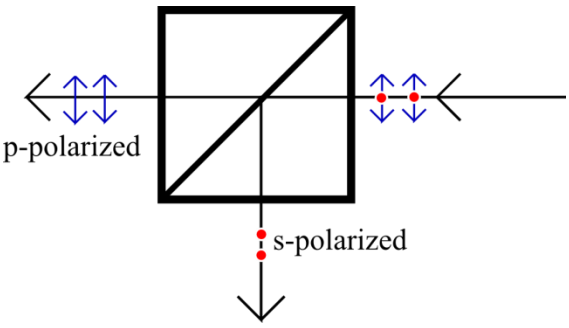

Fig. 3.4: The functioning of a polarizing beam splitter cube (PBS). Light polarized in parallel to the plane of incidence is transmitted, its perpendicular polarization component is reflected.

The sequences of a half-wave plate followed by a PBS, a quarter-wave plate and another half-wave plate played the role of, in terms of repeatable adjustment procedure, more reliable polarization controllers and were used to achieve good polarization overlap at the output fibre couplers for the sake of high visibility.

3.2.2.3 Polarization Controllers

Fibre polarization controllers, also called bat ear controllers, are simple devices consisting of a sequence of fibre coils that effectively reproduces a sequence of crystal wave plates. When looped, the mechanical stress in the fibre produces birefringence and consequently introduces a phase difference between the two orthogonal linear polarization components of the passing light; given a certain diameter of the loop, the number of fibre loops in one coil corresponds to the effect of passing through a quarter or half-wave plates. As with the bulk polarizing elements described in the previous section, by rotating in turn each of the sequence of $\lambda/4$ - $\lambda/2$ - $\lambda/4$coils enabled us to create an arbitrary polarization state from any incoming polarization state and thus optimize polarization dependent transmission through various components (polarizers and phase modulators).

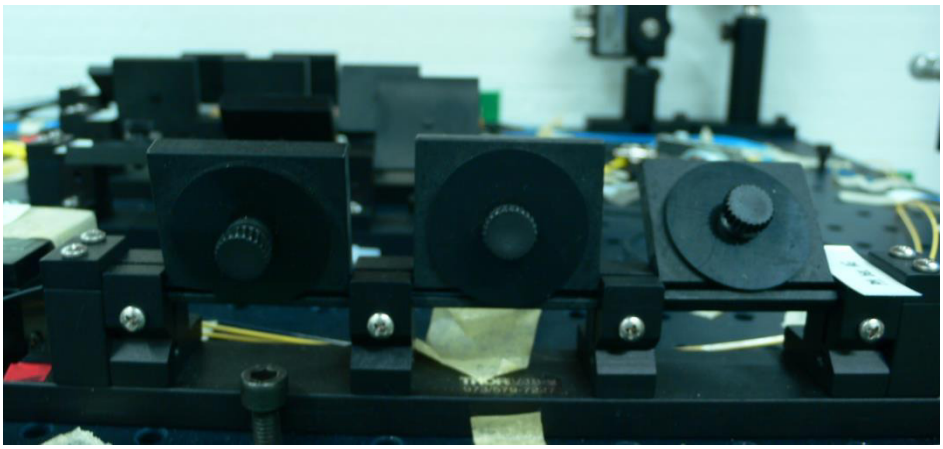

Fig. 3.5: Polarization controllers. The fibre is looped in a pre-manufactured plastic holder that enables rotation of the coils around its main axis.

3.2.2.4 Fibre Couplers

Fibre couplers are integrated optical devices which collect light from two or more input fibres and split it again between two or more output fibres, using different technology to achieve power redistribution, for example fusing of the fibres as with the ones in our

experiment. We only used 2-by-2 couplers where they played the role of beam splitters and enabled us to implement two intertwined Mach-Zehnder interferometers and perform projective measurement at the outputs. Our setup featured both fixed and variable ratio couplers (FCs and VRCs, see Fig. 3.2 above), although the option of splitting ratio adjustment was only availed of with the VRC at the output of the target qubit when we wanted to change the measurement basis. The splitting ratio was changed manually; we measured *T* in the following three bases: $\left\{\frac{1}{\sqrt{2}}(|0,1\rangle \pm|1,0\rangle)\right\}$, $\left\{\frac{1}{\sqrt{2}}(|0,1\rangle \pm i|1,0\rangle)\right\}$ and $\{|0,1\rangle, |1,0\rangle\}$, so three different splitting ratios were used: 50:50 (first two bases), 0:100 and 100:0 (the last basis). The fixed ratio couplers we used were made by SIFAM Fibre Optics and the variable ratio ones were manufactured by Canadian Instrumentation and Research Ltd. For more information on the particular types and serial numbers of FCs and VRCs, see Section 5.11 in [6].

3.2.2.5 Phase Modulators

Phase modulators (see Fig. 3.6 below) were key components to the operation of our setup. They enabled us to rotate the state of the source qubit around the equator of the Bloch sphere (add a phase factor between its basis states), change the measurement basis (see previous section), perform the feed-forward correcting operation (see Section 3.2.1.9 below), determine the visibilities of the interferometers and execute an active stabilization procedure (see the measurement description below). Phase modulators are electro-optical devices that employ the linear Pockels effect to modulate the phase of the light passing through by means of applied voltage: the refractive index of the crystal inside the modulator grows linearly with applied electric field. In this way, they are able to create a controlled path delay of the order of a wavelength.

In order to manipulate the phase with precision, we needed to know the proportionality between applied voltage and resulting path delay; this information is provided by a quantity called half-wave voltage – the voltage necessary to induce a phase shift ofπ. The half-wave voltages had already been determined in the previous experiment (see section 5.6 in [6] for the values of half-wave voltages, transmission losses and serial numbers of the products). However, half-wave voltage is in general different for different wavelengths and polarization states due to birefringence. All modulators we employed in

our setup (labelled as PM in Fig. 3.2 above) were made by EOSPACE with polarization maintaining fibres and two of them were equipped with integrated polarizers (labelled PMP). To allow for their optimization for transmission, they were preceded by polarization controllers (see Section 3.2.1.3 above) that could be rotated to obtain an arbitrary polarization state and thus achieve minimum loss of power due to transmission through the modulators. Another useful feature of the phase modulators is their speed; they are able to operate on frequencies of the order of tens of GHz[6].

The modulators were controlled electronically via a PCI-1723 multiple channel analog output card by Advantech.

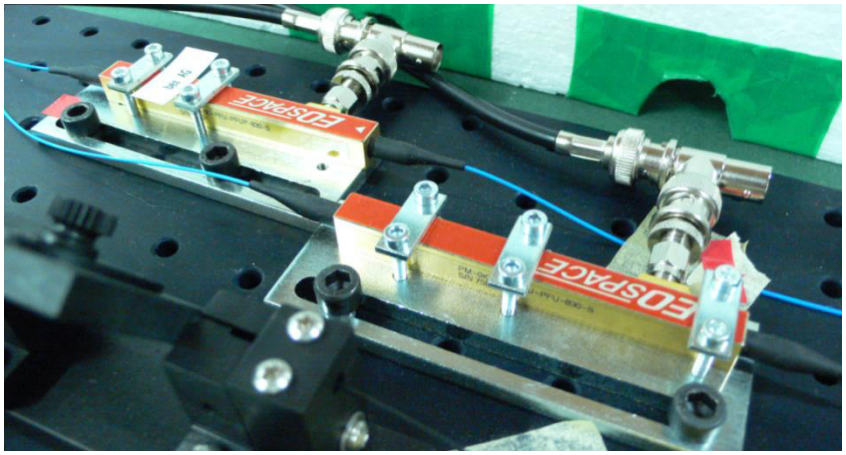

Fig. 3.6: Phase modulators (made by EOSPACE).

3.2.2.6 Detectors

As it was explained in Section 3.2.1.1 above, our setup operated in both a weak and a strong signal regimes: strong infrared laser diode signal served to adjust the setup, the same attenuated source was used for readjustment and stabilization during measurement and the weak down-converted signal was key to the actual measurement. Consequently, we also employed two types of detectors: PIN photo diodes when adjusting the setup with the probe diode and single-photon detectors in the weak signal regime. During setup adjustment, data from the PIN diodes were visualised in real time by means of an oscilloscope (WavePro 715Zi by LeCroy); it proved particularly useful when programmed for direct display of the visibilities.

[6] This is helpful for feed-forward applications.

The single-photons detectors in our experiment were silicon Geiger-mode avalanche photo diodes (APDs) – SPDCs (single photon counting modules) made by Perkin Elmer Optoelectronics. APDs are based on semiconductor physics and photoelectric effect: single photons trigger the injection of photoelectrons or holes that are subsequently accelerated and multiplied to produce a detectable electric signal; the avalanche process is then either quenched electronically or controlled by a load resistance. The SPDCs we used output positive TTL 4.5 V pulses. Due to their high sensitivity, the detectors have to be protected from normal lighting conditional when operating. To be able to work with the APDs, three important parameters had to be determined for the successful implementation of the measurement procedure: relative efficiencies, dark counts and the duration of detector response[7]. Relative efficiencies as well as dark counts (counts generated mainly thermally) had to be known and counted in our measurement results where applicable. The duration of detector response was essential to the setting of the coincidence logic and successful feed-forward operation (see Sections 3.2.1.8 and 3.2.1.9 below). The particular values of these parameters for the detectors we used can be found in section 5.8.2 in [6].

3.2.2.7 Counters

The pulses from detectors were collected and counted by counters controlled and read electronically from the computer via serial ports. However, they had first to be converted from TTL logic to NIM negative pulses; this was accomplished by means of an inverting transformer. We used two four-channel (Quad – model 974A) and one two-channel (Dual) Ortec CCNIM modules, that is, we had 10 channels altogether on our disposition, one of which played the role of timer; the first Quad module counted detections from detectors D_{a0}, D_{a1}, D_{d0} and D_{d1}, the second was used to count coincidences between each source and target qubit output detector pair and the two Dual module channelsserved to count coincidences between output detector pairs D_{a0}, $D_{a1}$and D_{d0}, D_{d1} for the measurement of Hong-Ou-Mandel dip (see Table 3.7 below for an overview).

[7] The overall delay between the impact of the photon and the production of an output TTL pulse.

QUAD				QUAD2				DUAL	
CH0 (ch.1)	CH1 (ch.2)	CH2 (ch.3)	CH3 (ch.4)	CHO (ch.5)	CH1 (ch.6)	CH2 (ch.7)	CH3 (ch.8)	CHA (ch.9)	CHB (ch.10)
c.r.	c.r.	c.r.	c.r.	coinc.	coinc.	coinc.	coinc.	coinc.	coinc.
D_{d0}	D_{d1}	D_{a0}	D_{a1}	D_{a0}-D_{d0}	D_{a0}- D_{d1}	D_{a1}- D_{d0}	D_{a1}- D_{d1}	D_{d0} - D_{d1}	D_{a0} – D_{a1}

Table 3.7: Overview of the counter channels usage. Ch. – channel, c.r. – count rate, coinc. – coincidences.

3.2.2.8 Coincidence Logic

In order to be able to count coincidences between the detectors, coincidence logic had to be employed. The coincidence logic produces pulses only if two arriving signals fall into a pre-defined time window. In our experiment, we used a passive delay module, a discriminator and a linear fan out together with a quad four-fold majority logic unit, all from Phillips Scientific (see Section 5.9.2 in [6] for more information). To set up the coincidence logic, we first had to determine the arrival time of individual pulses coming from the four detectors, counting in the detector response time (see previous section) and length of the coaxial cable. We then optimized the logic for maximum coincidence rate by changing the delay and narrowing down the coincidence window to ca 2.5 ns.

3.2.2.9 Feed-forward

The corrective feed-forward procedure served for rotating the state of the target qubit by π around the Bloch sphere, that is, multiply the state $|1,0\rangle_T$ by (-1) (see Section 3.1.3) in the case when a count was registered at detector D_{d1}, thus indicating that measurement on *S* yielded the result $|-\rangle$ which meant that the consequent state of *T* had to be corrected to obtain (3.5). This was done by conveniently using the TTL pulse from detector D_{d1} that, passing through a voltage divider, was applied directly to the phase modulator PM_π (see Fig. 3.8 below) where feed-forward corresponds to the operation U_π). The voltage divider was set in a way to modify the TTL pulse to the value of the half-wave voltage of PM_π. See [5] for more information (for example, timing and half-wave voltage measurement) on the technique.

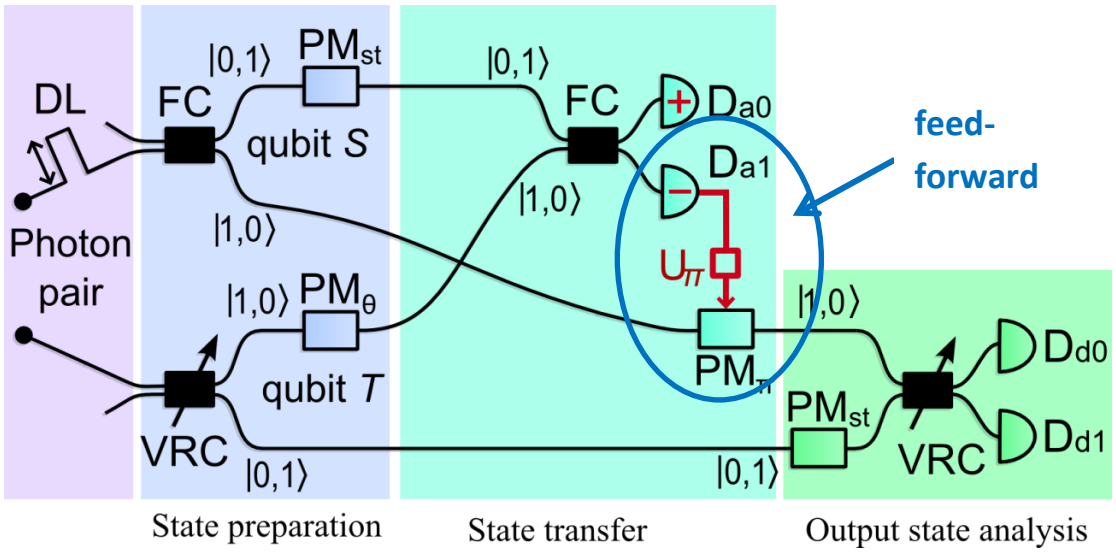

Fig. 3.8: Scheme of the setup in Fig. 3.1 showing the feed-forward mechanism.

3.2.3 Setup adjustment

Before any meaningful measurement could be carried out, the setup had to be adjusted to its optimum performance. This was done in several steps with the use of the strong infrared probe diode signal that could be monitored in real time on an oscilloscope. First, the setup had to be adjusted to induce minimum transmission losses; second, both interferometers had to be optimized to reach maximum visibility.

1. Optimizing coupling of the air gaps

   In order reach the first goal, before routine setup adjustment, transmission through the air gaps in each of the interferometer arms was checked and coupling on the output side was optimized.

2. Minimizing transmission losses

   Next, transmission through the polarizers placed before the input fibre couplers (see Section 3.2.1.2) had to be maximized. This was done by means of polarization controllers placed before the polarizers - the rotation of the “ears” of the fibre polarization controllers produces the same effect as the rotation of a bulk wave plate (see Section 3.2.1.3).

3. Compensating losses for high visibilities

   In order to reach maximum visibilities, we had to have equal intensities arriving at the output beam splitters. Therefore, losses in both interferometers had to be compensated

for; this was done by inducing losses by means of polarization controllers in the stronger arms. For more detailed treatment of the losses, see Section 4.1 in [6].

4. Maximizing polarization overlap for high visibilities

Besides intensity, the quality of interference depends on the polarization state of interfering light. Polarization in both arms of the two interferometers thus had to overlap. This was secured by adjusting the polarization via a sequence of polarizing components in the inner rails of the interferometers (green and orange arms in Fig. 3.1).

5. Compensating optical paths for high visibilities

We have supposed here that the optical paths in both interferometer arms had been balanced from previous operation of the setup. If interference had not been observed in the latter two steps, air gap lengths in one of the interferometers arms would have had to be manually adjusted and consequently, the whole procedure starting from 3. would have had to be repeated. Nevertheless, compensation of the path difference with full accuracy constituted the last step of the whole procedure. When visibilities had been maximized by balancing the intensities and securing polarization overlap, the air gaps in the outer rails of the interferometers (in blue and yellow in Fig. 3.1) were scanned by means of motorized translation stages on which the output coupling lenses were placed and a computer-run programme that would compare the resulting visibilities at each position of the stage (the length of scan step was chosen according to our needs) and send the stage to the position of the highest visibility.

In between measurement sessions, the setup, considered approximately optimized, could be alternatively adjusted using the probe diode in a weak mode, attenuating its power to cca a million photons per second (resulting in numbers of photons at each output detector revolving around hundred or two hundred thousand per second).

4 Measurement

When the setup had been adjusted, the measurement process itself consisted of one optional manual and three computer-run procedures operated via Matlab. The manual setting of the measurement basis (see Section 3.2.1.4) by changing the output fibre coupler splitting ratio depended on whether we wanted to perform the measurement of *T* in one of the two bases $\left\{\frac{1}{\sqrt{2}}(|0,1\rangle \pm |1,0\rangle)\right\}$ and $\left\{\frac{1}{\sqrt{2}}(|0,1\rangle \pm i|1,0\rangle)\right\}$ that required a splitting ratio of 50:50 or in the basis $\{|0,1\rangle, |1,0\rangle\}$ which required a splitting ratio of 0:100 and 100:0. The π phase factor for the second basis was added later in the course of the electronic routine.

The purpose of the first Matlab routine was to set the optical paths lengths in both interferometers to zero delay between two photons arriving at the output fibre coupler with respect to a reference position of the motorized stage present in the source (see Section 3.2.2.1), that is, in other words, set the motorized air gaps in the outer rails of the interferometers (see Fig. 3.1) to a length corresponding to the HOM dip minima. The HOM dips minima for both interferometers would then coincide if we measure them using the motor in the source. The routine measured the HOM dip at both outputs of the two interferometers, recorded data about the shape of the dip with respect to specific motor positions and set the motors in the air gaps to the positions of dip minima. When the interferometers had been set to perfect time overlap of arriving photons, the HOM dip was scanned once more, this time using the motor in the source, to acquire data about the shape and size of the dip. The second Matlab routine thus performed a similar scan of the dip as the first one, this time fitting the data, recording fit parameters and setting the motor to the reference position again. Let us note here for clarity that we used motorized stages inside the setup for the adjustment of path lengths whereas the motorized translation stage inside the source served to record information about the dip and move within the dip during the actual measurement.

When the interferometers had been set to HOM dip minima and information about the dip had been acquired, the main measurement routine could be started. This included a set of 3-second-long measurements of coincidence rates for a preset number of positions in the HOM dip (corresponding to the delay between the source and target qubits), a number of phases of the source qubit and three measurement bases as indicated above. Each single

measurement in the set was followed by a stabilization procedure that insured that the phase in both interferometers hadn't drifted and corrected the drift when needed.

4.1 First Scan of the HOM Dip

The scan routine had to communicate with the analog and digital input/output cards that controlled the motors and the choppers (respectively) and also with the counters; it measured coincident counts in a given range, that is, at a given number of positions of the motors around a specified central positions (approximately corresponding to HOM dip minima known from previous test measurements). The measurement at each of the positions recorded coincidences for 20-150s, according to the precision needed. When the scan had been finished, the routine would set the air gaps to a length which corresponded minimum coincidence rate and thus to a perfect time overlap of the photons at the output fibre coupler (to the HOM dip minimum – see Fig. 3.9 below).

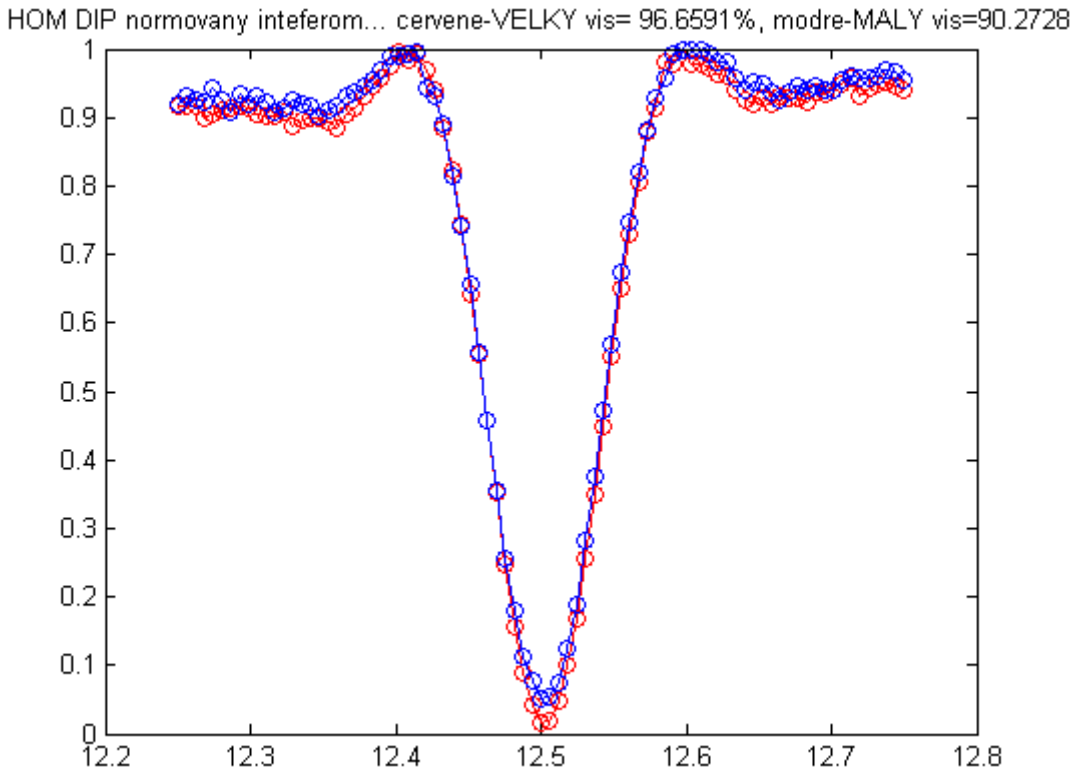

Fig. 3.9: Normalized HOM dip measured at the two interferometers (measurement time here was 150s at each motor position). The visibility of the dip measured at the output of the target qubit was approximately 97% whereas the visibility of the dip measured at the source qubit was lower by a few percent. We used data from dip measurement at the target qubit for that reason.

Before the scan, it had to be made sure that the choppers in the source were set to transmit the down-converted photons and not the infrared laser diode. A simple procedure based on count rate measurements tested the choppers for transmission and set them to the right position. This was necessary because of the choppers having no identifiable numbered positions: when an electric pulse (TTL) is sent on the chopper, it makes it rotate by a fraction of the whole turn so that it either blocks or unblocks the beam (see Fig. 3.10 below). The test was performed to find out its current position. One chopper was placed right after the blue laser, another right after the probe diode, so the procedure tested both in sequence.

A simplified scheme of the HOM dip scan routine is given here below. The inputs variables of the routine function were: *number of motor positions, scan range* (the scan was performed in the range 2*half scan range around the central positions specified).

HOP_dip_scan(central_position_source, central_position_target, half_scan_range, number_of_motor_positions)

```
initialize analog output card
initialize digital output/input card
initialize counters
initialize motors
measurement_time=20s[8]
create position_vector_source, from(central_position_source - half_scan_range) to (central_position_source + half_scan_range), with step 2*half_scan_range/number_of_motor_positions
create position_vector_target, from(central_position_target - half_scan_range) to (central_position_target + half_scan_range), with step 2*half_scan_range/number_of_motor_positions
test choppers for transmission
block probe diode, unblock SPDC photons
for j=1:number_of_positions
      for int=source:target
            send motor to position: position_vector_int(j)
      end
      count coincidences for measurement_time
```

[8] Was varied later, with longer measurement time for better precision.

```
        save counts to file (i, motor_position_source, counts_source,
        error_source, motor_position_target, counts_target,
        error_target)
end
fit measured data
save fit parameters to file
visualize data
send motors source and target to the position of minimum counts
close all communication channels
```

For the full programme code, please see part 1 of the Appendix.

4.2 Second Scan of the HOM dip

In the case of the first two measurement bases, the HOM dip was measured at both interferometers outputs; in the case of the last one, it was only measured at the source qubit output (consequently, only the source qubit interferometer was stabilized during the measurement). The routine for the second scan was similar to the first one (see above for a simplified scheme of the programme), but employed only the motor mounted in the source. Coincidences were measured at each position of the motor for between 30 - 150s – higher measurement time ensured a reasonable error to half-maximum count rate ratio with regard to the Poisson uncertainty $\sqrt{n}$ where *n* is the number of counts and consequently a reliable fit of the data acquired (around 3000 coincidences out of the dip, see Fig. 3.11 below). The measurement time was recorded in an auxiliary file for the scaling of data in the main measurement routine where a different measurement time duration could be convenient. The data acquired about the shape and positions of the HOM dip were fitted and the fit parameters saved to be employed in the main measurement routine. A parabolic fit was used in the area around the minimum of the dip, linear curves were used to fit the sides (see Fig. 3.11). For the full programme code, see part 2 of the Appendix.

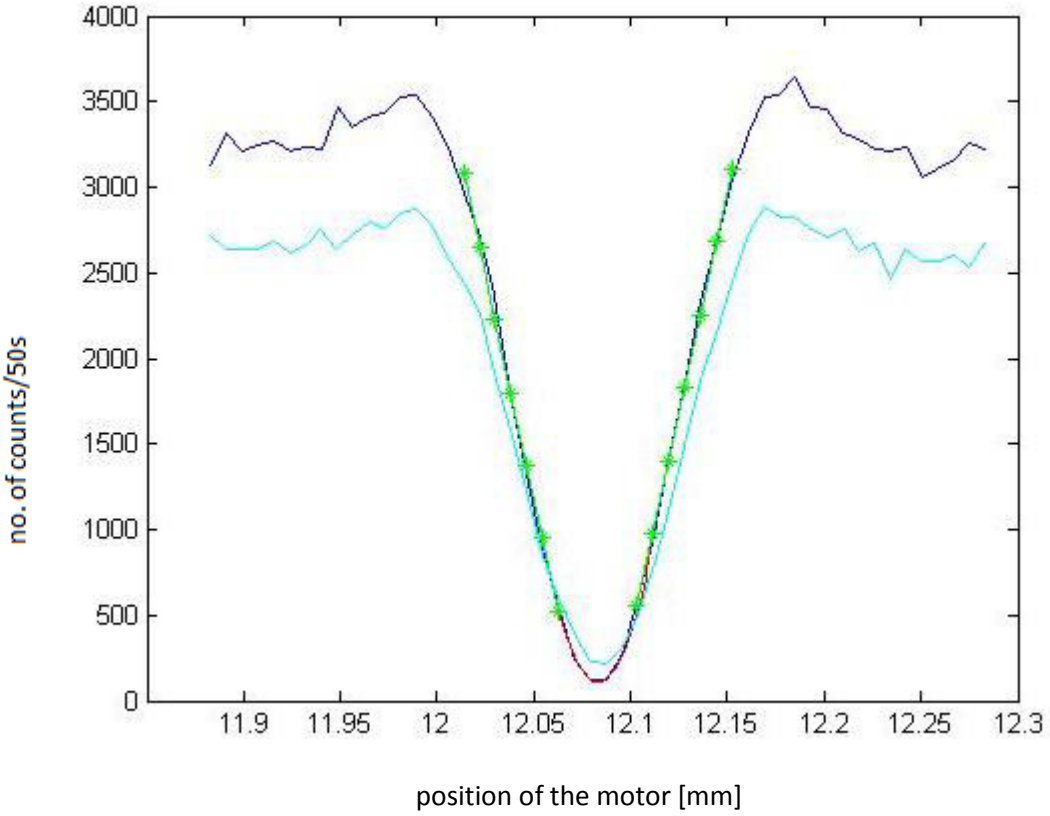

Fig. 3.11: HOM dip measured at the output of the two interferometers, showing the number of counts per 50s at different positions of the motors and a fit of the resulting curve with two linear functions for the sides and one polynomial function for the area around the minimum of the dip.

4.3 Main Measurement Routine

As it was summarized above, the main measurement routine consisted of 3-second-long measurements of coincident counts between each pair of detectors (see Table 3.7 for overview), each measurement followed by a stabilization procedure and carried out for: 1) a preset number of positions along the HOM dip corresponding to a delay between the source and target photons, 2) a number of phases appearing with the input state of the source qubit and 3) three measurement bases for subsequent quantum state tomography of the target qubit. The routine needed the data acquired and saved by the second HOM dip scan programme to operate; this is why it had to be run before the measurement. Based on the parameters acquired by the previous routine, the programme moved to a specific position in the dip and counted coincidences between all the detectors for each of the number phases

of *S* specified as inputs of the programme[9], stabilizing the interferometers after every 3s of measurement. This was first repeated at each of the positions within the dip for the first two bases, then the splitting ratio of the output beam splitter was reset to 0:100 (or 100:0) and the routine was run again. Stabilization was carried out in the weak (attenuated) probe laser diode regime; as visibilities had to be known for the stabilization process, they were measured, before each set of measurements at a certain position in the dip, also by means of the probe diode. If, for some reason, visibilities were found to have decreased considerably, as high values were preferable, an automatic procedure would rescan the air gaps inside the interferometers and reset the optical path length to improve them. A number of corrective measures were taken throughout the measurement to allow for motor error, fluctuations of intensity and optical path drift to make sure that the measurement was performed for the correct value of delay between the photons (at the correct position in the dip) and in this way guarantee its precision (see blue commentary in bold in the programme scheme below). A simplified scheme of the whole routine is given here below. For the full programme code, see part 3 of the Appendix. As explained above, the inputs of the main measurement programme were: number of positions in the dip, number of phases of S, splitting ratio, number of cycles of measurements to be performed for each phase, interferometers to be stabilized (1 – target qubit; 2 – source qubit, 3 – both interferometers).

Note: as in the previous routines, at the beginning of the main measurement programme, the choppers had to be tested for transmission in order to get a reference transmission and block position (see 3.3.1 above).

```
MAIN_MEASUREMENT(number_of_dip_positions, number_of_S_phases,
splitting_ratio, number_of_cycles)
specify measurement times: probe=0.1s
                           SPDC_photons=3s
                           choppers_test=1s
                           dip=100s
```

[9] In fact, we performed a set of measurements for all the phases twice to average over the two ensembles: once applying a positive phase to the modulator PM_θ and again applying a negative phase to the modulator PM_{st} in the outer rail of the source qubit interferometer, as both of these operations lead equivalently to the multiplication of the state $|1,0\rangle_S$ by a phase factor $e^{i\theta}$.

```
if splitting_ratio==50, max_faze_out=1, elseif splitting_ratio==100,
max_faze_out=0; %the measurement basis with 0:100 or 100:0 does not
include a phase factor[10]

initialize analog output card

initialize digital output/input card

initialize counters

initialize motor in the source

create file for later saving of data

set measurement_time to choppers test

test choppers for transmission

block probe diode, unblock SPDC photons

read data for measurement: background and dark counts, half-wave
voltages, HOM dip parameters (fit parameters and positions of
minima)

%dip parameters:

x_half_intensity      %highest derivation point

half_intensity_orig   %original coincidence rate at the highest
                      derivation point

max_intensity_orig=2*half_intensity_orig

dip_measurement_time  %measurement duration, scale reference for
                      intensities

parabol_limit         %intensity limit for the application of the
                      parabolic fit

minimum_cr_target[11]    %count rate at the HOM dip minimum

minimum_target        %position of HOM dip minimum

maximum_target        %position of HOM dip maximum

delta_x=0             %dip minimum position, cumulates all drift

%fit parameters:

right_slope_target    %linear fit tangent

lin_ofset_target

for d=1:number_of_dip_positions
```

%check of the precision of dip position calculation and corrective measure for recalculation to account for dip drift with respect to the motor position and intensity fluctuations:

[10] The sign % denotes comments without operational value.

[11] „Target" refers to the dip measured at the output of the target qubit interferometer.

```
if splitting_ratio==50 %only meaningful in the case of the
first two bases
      set measurement_time to dip[12]    %100s
      send motor to position maximum_target+0.3[13]
      measure intensity=max_intensity %measure new maximum
      intensity out of the dip
      error=sqrt(max_intensity); allowance=2*error
      half_intensity=max_intensity/2
      save max_intensity to file
      corr_intensity= max_intensity_orig/max_intensity
      %corrective factor to account for intensity fluctuations
      send motor to position x_half_intensity
      measure intensity=I
      correction=0;
      %corrective measure:
      if intensity ϵ (half_intensity+-allowance) &&
      correction=<1
       while intensity ϵ (half_intensity+-allowance)
       delta_x=delta_x+((I- half_intensity)*corr_intensity)/
       right_slope_target
       send motor to position x_half_intensity-delta_x
       save delta x to file, measure intensity
       if intensity ϵ (half_intensity+-allowance)
       correction=correction+1   %the calculation is only
       corrected once
       end
       end %while
      else
       delta_x=delta_x+0
      end %if intensity lies in the tolerance interval
end %if splitting_ratio==50, end of the check and correction
```

```
%dip position calculation:
int_position=(d-1)*(maximum_intensity/(number_of_dip_positions-
1))
%with the position given, we should measure this intensity
if int_position==0
```

[12] We used high measurement times for precise calculation of the position in the dip.
[13] In reality, when before each motor move, we included an extra move to a position displaced by 0.2mm from the target position to account for motor hysteresis.

```
      send motor to position minimum_target-delta_x
elseif abs(int_position-maximum_intensity)<=
(maximum_intensity*0.001)
      send motor to position minimum_target-delta_x+0.3 %off
      the HOM dip edges,[14]
else
      if int_position<=
      (min_cr_target/dip_measurement_time)*measurement_time
            use the parabolic fit to calculate delta_x
      else
            use the linear fit to calculate delta_x
      end
      send motor to position:
      ((int_position*corr_intensity- lin_ofset_target)/
      right_slope_target)- delta_x
end
      block SPDC photons, unblock probe diode
      measure visibilities (improve if necessary)
      block probe diode, unblock SPDC photons
for faze_out=0:max_faze_out
      for qu=1:2[15]
            for f=1:number_of_S_phases
                  for cycle=1:number_of_cycles
                  block SPDC photons, unblock probe diode
                  stabilize interferometers
                  block probe diode, unblock SPDC photons
                  set phase of source qubit
                  set phase_out of the measurement basis
                  measure coincidences
                  save data to file
                  delete phase
                  end %for number_of_cycles
            end %for number_of_S_phases
      end %for qu
end %for faze_out
```

[14] We measured the "raised shoulders" of the HOM dip separately later.
[15] Measurements were performed for all the phases twice, see footnote 2).

```
end
close all communication channels
```

4.4 Active Stabilization

Our setup was mounted on an optical table and isolated in a polystyrene box. However, this passive way of stabilizing the experiment was not sufficient to prevent phase drift to which it was prone, mainly due to optical fibres being especially sensitive to temperature fluctuations. This is why we employed a method of active stabilization of the interferometers based on the same principle as in [5] and [6] based on the routine proposed by Miloslav Dušek in [19] - in the case of drift, phase was repeatedly corrected by means of optical phase modulators.

4.4.1 Principle

After each 3s of measurement, the experiment switched to the probe laser diode regime and the stabilization routine checked whether the phase had drifted, comparing the current intensity measured to a reference intensity in the interference fringes; if the difference was found to be higher than a certain preset limit value, the amount of drift was calculated from the sinusoidal character of the visibility fringes (see Fig. 2.6 and Section 2.4) and a corresponding fraction of half-wave voltage was applied to correct for it. If phase in both interferometers was found to have drifted, both interferometers were stabilized; if one of the interferometers was found stable, only the other was stabilized. At the end of each corrective process, the phase in both interferometers was checked and the measurement could proceed only if both interferometers were stable[16]. A simplified scheme could be described as follows:

```
while interf_1 OR interf_2 are not stable
      if interf_1 AND interf_2 are not stable
            stabilize both simultaneously
      end
      for k=1:2
            if interf_k is not stable
```

[16] Naturally, stabilization of both interferometers was meaningful only in the case of 50:50 output splitting ratio; in the case of 0:100 or 100:0 splitting ratio, only the source qubit interferometer was stabilized.

```
                stabilize interf_k
            end
        end
end
```

4.4.2 Stabilization Routine

The stabilization routine applied a phase corresponding to a minimum in the interference fringes, measured counts and tested the normalized intensity acquired:

$$Y_0 = \frac{\mathrm{I}_0 - \mathrm{I}_{\max}}{\mathrm{I}_{\max} - \mathrm{I}_{\min}}, \qquad (3.6)$$

where I_0 are the counts just measured and $\mathrm{I}_{\max}$ and $\mathrm{I}_{\min}$ maximum and minimum intensities of the interference fridges previously measured at the detector, against a certain limit, which we chose to be $\mathrm{lim} = 0.006$.[17] Before measurement at each of the dip positions, a procedure measuring visibilities recorded counts at the detectors so that their index corresponded to the voltage applied at the phase modulators and saved the value of minimum and maximum intensities at both detectors into the variables I_{min} [18] and I_{max}. The stabilization routine then determined the value of voltage U_{min} corresponding to I_{min} and worked with these values: U_{min} was applied at the phase modulator that served for stabilization, counts were read from both detectors and the following ratios were calculated:

$$\mathrm{x}_0 = \frac{\mathrm{I}_0}{\mathrm{I}_{\mathrm{tot}}} = \frac{\mathrm{I}_0}{\mathrm{I}_{\mathrm{min1}} + \mathrm{I}_{\mathrm{max1}}}$$

$$\mathrm{x}_1 = \frac{\mathrm{I}_1}{\mathrm{I}_{\mathrm{tot2}}} = \frac{\mathrm{I}_1}{\mathrm{I}_{\mathrm{min2}} + \mathrm{I}_{\mathrm{max2}}}$$

where x_1 corresponds to the second detector and $\mathrm{I}_{\mathrm{tot}}$ is determined from previous visibility measurement.

One can easily check that

$$Y_0 = \frac{\mathrm{I}_0 - \mathrm{I}_{\max}}{\mathrm{I}_{\max} - \mathrm{I}_{\min}} = \left(\frac{\mathrm{I}_0}{\mathrm{I}_{\mathrm{tot}}} - \frac{1-\mathrm{V}}{2}\right).\frac{1}{\mathrm{V}} = \left(\mathrm{x}_0 - \frac{1-\mathrm{V}}{2}\right).\frac{1}{\mathrm{V}}$$

[17] This limit corresponded to a drift of approximately 1/40 of the full cycle.
[18] The description here is restricted to general variables for brevity; note that in the actual routine, corresponding variables I_{min11}, I_{min12}, I_{min21}, I_{min22} were calculated for both interferometers.

where V is the visibility given by 2.12.

However, to take into account possible intensity fluctuations, we also divided the quantity x_0 by the sum of $x_0 + x_1$ corresponding to intensities at both detectors, so y_0 was calculated as

$$y_0 = \left(\frac{x_0}{x_0 + x_1} - \frac{1 - V}{2}\right).\frac{1}{V}.$$

In principle, y_0 could be negative for very low values of $\frac{x_0}{x_0+x_1}$. This potential error was accounted for by a conditional correction that would reset the factor $\frac{1-V}{2}$ to the value of $\frac{x_0}{x_0+x_1}$.

If the normalized intensity y_0 did not satisfy the limit $y_0 < lim$, the phase in the interferometer in question was corrected until the condition was met. In the case, though, when a limit number of phase corrections had been carried out unsuccessfully, the stabilization routine would run a new visibility measurement procedure and redetermine all the variables needed for phase correction, eventually rescan the air gaps in the interferometers for better visibilities.

The phase drift α was determined by means of the inverse sine function, after a phase of $\pi/2$ had been applied and the new normalized intensity $y_{\pi/2}$ calculated, as

$$\alpha = \arcsin\left(2 * y_{\pi/2} - 1\right).$$

To take into account the two possibilities: either the phase has drifted by more or by less than a quarter of a wave, we reset the U_{min} in the following way:

```
if y0<=0.5
      Umin=Umin-(alpha/pi)*half_wave_voltage
else
      Umin=Umin-((pi/alpha)/pi)*half_wave voltage
end
```

The routine then applied the new U_{min} and remeasured intensities; if y_0 was now found to be under the limit lim, the interferometer in question was considered stabilized.

For the full programme code, please consult part 4 of the Appendix.

5 Results

We prepared two qubits (target – *T* and source - *S*) in the states:

$$|\Phi\rangle_T = \frac{1}{\sqrt{2}}\left(|0,1\rangle_T + |1,0\rangle_T\right)$$

and

$$|\Psi\rangle_S = \frac{1}{\sqrt{2}}\left(|0,1\rangle_S + e^{i\theta}|1,0\rangle_S\right),$$

respectively, executed state transfer from qubit *S* onto qubit *T* and measured qubit *T* at the output. We have carried out sets of 15 3-s measurements for 7 different values of θ: 0°, 30°, 60°, 90°, 120°, 150° and 180°[19], each in three different bases: $\left\{\frac{1}{\sqrt{2}}(|0,1\rangle \pm |1,0\rangle)\right\}$, $\left\{\frac{1}{\sqrt{2}}(|0,1\rangle \pm i|1,0\rangle)\right\}$ and $\{|0,1\rangle, |1,0\rangle\}$, for 16 values of delay Δt between the source and target qubit photons (16 positions in the HOM dip)[20].

For each Δt, the indistinguishability parameter *D* was calculated from the relative coincidence rate

$$R_{rel} = \frac{R(\Delta t)}{R(out)},$$

where *R*(*out*) was coincidence rate measured out of the dip and far enough from the "raised shoulders" of the dip (see Fig. 4.1 below). The raised area where R_{rel} is bigger than 1 thus correspond to a negative *D*; this indicates that $\rho_{E,ST}$ is not a factorable state and the environmental states of the qubits are entangled (see Section 3.1.3).

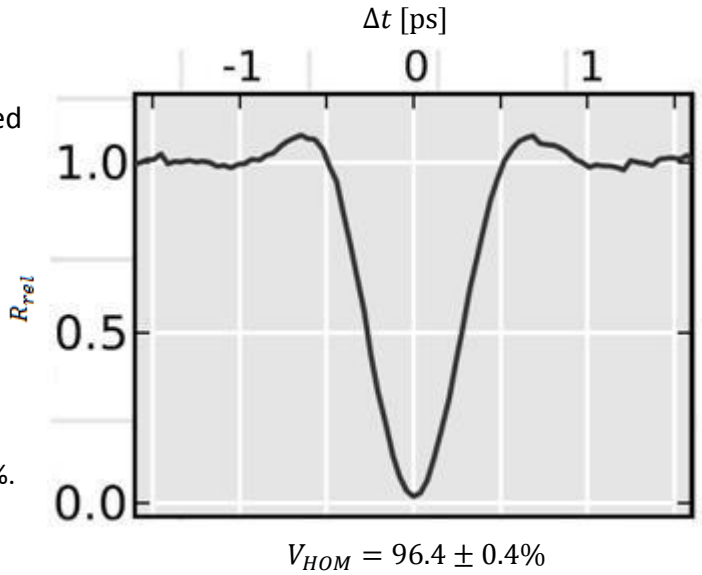

$$V_{HOM} = 96.4 \pm 0.4\%$$

Fig. 4.1: Normalized HOM dip. Relative coincidence rate plotted against time delay between the two photons. Relative measurement error in the minimum was 6%, in the maximum less than 2%. Visibility of the dip was approximately 96%.

[19] Averaging over two sets of measurements for each phase.
[20] The area of the „raised shoulders" of the dip and where *D* is around 0 or negative was measured in more detail.

Output density matrices ρ_T^{rec} were reconstructed using maximum-likelihood quantum tomography [20-21] and quantities characterizing the quality of the transfer such as purity, fidelity, eigenvalues and overlap of the output and input states were calculated from them. The theory predicts that the overlap of input (see (3.5)) and output state is equal to

$$\langle\Psi|_S\rho_T|\Psi\rangle_S = \frac{1+D}{2}$$

end the eigenvalues of ρ_T are $\frac{1+D}{2}$ and $\frac{1-D}{2}$. Fig. 4.2 shows experimental results and reveals good accordance with the theoretical prediction.

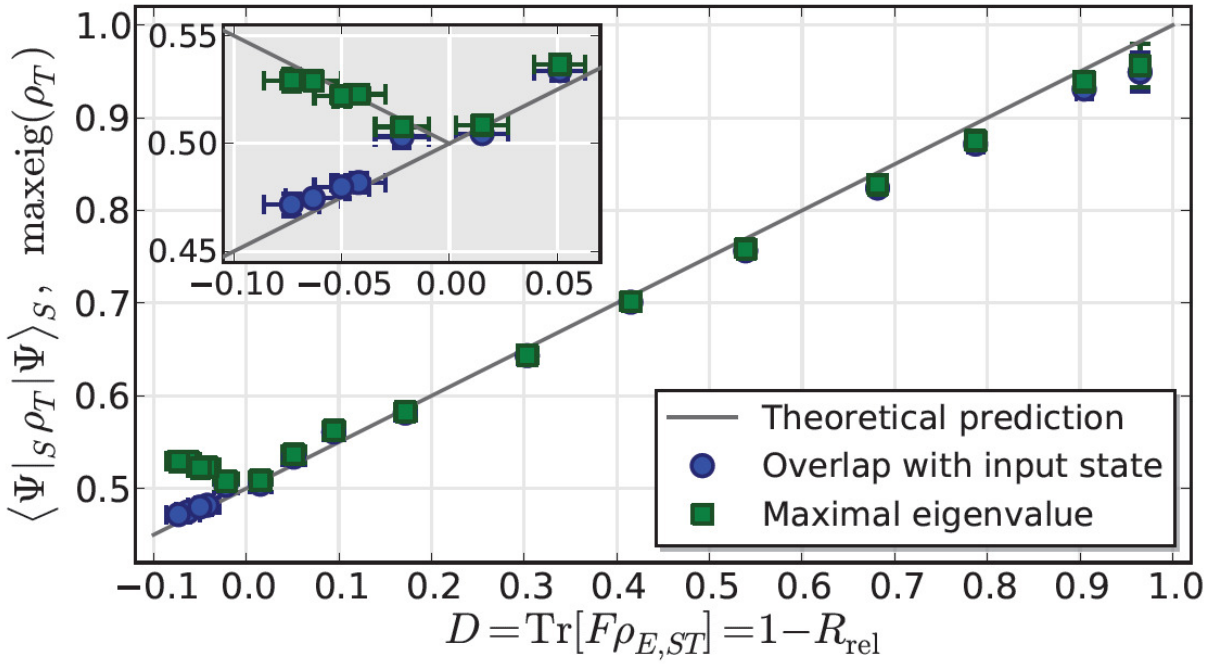

Fig. 4.2: Results of the experiment. Overlap of input and output states and maximum eigenvalues of the output state plotted against the indistinguishablity parameter *D*. Coloured squares show values obtained in the experiment, grey lines theoretical prediction. The area where *D* is negative or close to zero is magnified. Created by: Miloslav Dušek.

The average output state fidelity (with respect to the theoretical output state)

$$F(\rho_T, \rho_T^{rec}) = \left[Tr(\sqrt{\sqrt{\rho_T}\rho_T^{rec}\sqrt{\rho_T}})\right]^2$$

was calculated to be $99.2 \pm 0.8\%$.

Conclusion

We have successfully tested a directly measurable parameter quantifying effective indistinguishability of quantum particles that is especially relevant in quantum information protocols where indistinguishability represents an important resource. Unlike overlap, the indistinguishability parameter proposed here is valid for both factorable and non-factorable states. It is defined by means of a flip operator that effectuates a partial exchange of non-informational degrees of freedom of the particles. The results obtained proved a direct dependence of the quality of information transfer on the parameter proposed.

The experimental test was a quantum state transfer protocol based on the HOM effect, realized in a linear fibre-optical setup where qubits were carried by photons generated by parametric down-conversion; their basis states were represented by optical spatial modes. The setup used was based on the implementation of a programmable phase gate with 50% success probability [18] consisting of two intertwined fibre Mach-Zehnder interferometers. The state transfer was carried out by a swap of two rails between the interferometers and subsequent projective measurement on one of the qubits. All measurement was computer-run via programmes written in Matlab and the output state was reconstructed using quantum state tomography. Various measures of the quality of state transfer were calculated and theoretical predictions of their direct dependence on the indistinguishability parameter were confirmed.

The significance of this experiment lies in the general operational quality of the parameter proposed. However, the collective effect of multiple resources in more complicated protocols where indistinguishability is not the only key information processing quality factor is yet to be investigated.

References

[1] M. Miková, H. Fikerová, I. Straka, M. Mičuda, M. Ježek, M. Dušek and R. Filip, Carrying qubits with particles whose noninformational degrees of freedom are nonfactorable. Phys. Rev. A 87, 042327 (2013)

[2] M. A. Nielsen and I. L. Chuang, *Quantum Computation and Quantum Information.* Cambridge University Press, 2010.

[3] M. Dušek, *Koncepční otázky kvantové teorie*, UP Olomouc, 2002.

[4] P. Kaye, R. Laflamme, M. Mosca, *An Introduction to Quantum Computing*, Oxford University Press, 2007.

[5] H. Fikerová, *Bachelor's Thesis: Optical Setups for Quantum Information Processing*, Department of Optics, Palacky University in Olomouc, 2010.

[6] M. Miková, *Diploma Thesis: Optical implementation of quantum operation for quantum information processing using entangled photons: APLICATION OF ELECTRONIC FEED-FORWARD,* Department of Optics, Palacky University in Olomouc, 2011.

[7] T. S. Metodi, A. I. Faruque,F. T. Chong, *Quantum Computing for Computer Architects*, Morgan & Claypool, 2011, p.53.

[8] E. Knill, R. Laflamme and G.J. Milburn, *A scheme for efficient quantum computation with linear optics*, Nature, Vol. 409 (Jan. 4, 2001)

[9] I. Straka. Diploma Thesis: Optical frequency conversion and non-classical light generation, Department of Optics, Palacky University in Olomouc, 2012.

[10] C. C. Gerry and P. L. Knight, *Introductory Quantum Optics*, Cambridge University Press, 2005.

[11] A. Peres, *Quantum Theory: Concepts and Methods*, Kluwer Academic Publishers, 2002.

[12] L. Del Debbio, *Lectures on Quantum Mechanics*, http://www2.ph.ed.ac.uk/~ldeldebb.

[13] P. Kok, *Lectures*. http://www.pieter-kok.staff.shef.ac.uk/.

[14] L. Mandel and E. Wolf, *Optical Coherence and Quantum Optics* (Cambridge University Press, Cambridge, 1995).

[15] C. K. Hong, Z. Y. Ou and L. Mandel, *Theory of parametric frequency down conversion of light,* Phys. Rev. A 31, 2409-2418 (1985)

[16] M. W. Hamilton, *Phase shifts in multilayer dielectric beam splitters*, Am. J. Phys. 68, 186 (2000)

[17] C. K. Hong, Z. Y. Ou and L. Mandel, *Measurement of Subpicosecond Time Intervals between Two Photons by Interference*, Phys. Rev. Lett. 59, 2044-2046 (1987).

[18] M. Miková, H. Fikerová, I. Straka, M. Mičuda, M. Ježek, M. Dušek, *Increasing efficiency of a linear-optical quantum gate using an electronic feed forward*, Phys. Rev. A 85 012305 (2012).

[19] M. Dušek, *Aktivní stabilizace interference* (Protocol), Department of Optics, Palacký University in Olomouc, 1997.

[20] Z. Hradil, *Quantum-state estimation*, Phys. Rev. A 55, R1561 (1997).

[21] M. Ježek, J. Fiurášek and Z. Hradil, *Quantum inference of states and processes*, Phys. Rev. A 68, 012305 (2003).

1. MATLAB routine for the first scan of the HOM dip (see Section 4.1)

```
%%%%%%%%%%%%%%%%%%%%%%%%%%%%%%% MERENI_2DIPU %%%%%%%%%%%%%%%%%%%%%%%%%

function []=MERENI_2DIPU(stred_motor_velky, stred_motor_maly, plus_minus_delka_scanu,
pocet_mereni_dipu)

%-----------------------pevne nastavene parametry---------------------
port  = 'COM1'; %komunikace s quadem
port2 = 'COM2'; %komunikace s quadem2
port3 = 'COM3'; %komunikace s motory
port4 = 'COM6'; %komunikace s dualem

casova_zakladna='s';
doba_mereni=20;
inic_motoru
inic_karet_dio %vytvori objekt dio na komunikaci s kartou a vytvori vektora_dio [0 0 0
0] V
inic_counteru  %Q2ext_D1 - inicializuji se QUADY s externi casovou zakladnou a DUAL
dual_nastaveni
det_ucinnosti; %dektekcni ucinnosti APD

%promenne:
dip=[];
datum=clock;
den=datum(3);
mesic=datum(2);
casek=datum(4)*60 + datum(5);

%%%%%%%%%%%%%%%nastaveni zapisovani vysledku do souboru%%%%%%%%%%%%%%%%%%%%%
soubor=['HOMdipy.dat'];
fid=fopen(soubor, 'a'); %pripis do puvodni souboru
fprintf(fid, ['\n Mereni HOM dipu z ' num2str(datum(3)) '.' num2str(datum(2)) '.'
num2str(datum(1)) 'v ' num2str(datum(4)) 'h. ' num2str(datum(5)) 'min.']);
fprintf(fid, ['\n SOUBOR: poradi, poloha_motor_velky, coinc_velky,
chyba_coinc_velky_dip, poloha_motor_maly, coinc_maly, chyba_coinc_maly_dip' '\n']);
fclose(fid);

soubor1=['HOMdipy_minima.dat'];
fid1=fopen(soubor1, 'a'); %pripis novych hodnot
fclose(fid1);

%%%%%%%%%%%%%%%%%%%%%%%%%%%%%%%%MERENI%%%%%%%%%%%%%%%%%%%%%%%%%%%%%%%%%%%%

velky_m =linspace((stred_motor_velky - plus_minus_delka_scanu),(stred_motor_velky +
plus_minus_delka_scanu), pocet_mereni_dipu);
maly_m =linspace((stred_motor_maly - plus_minus_delka_scanu),(stred_motor_maly +
plus_minus_delka_scanu), pocet_mereni_dipu);
pojezd=[velky_m; maly_m];
pause(0.5)
test_pruchodnosti_vrtulek  %nastavi obe VRTULKY na pruchod do experimentu
pozice=3; %PARY (modry laser) odkryte, PROBE (cerveny laser) zakryty; vrtule c.3
puls_x %otoceni vrtuli c. 3 -> cerveny svazek zastinen

for j=1:pocet_mereni_dipu

    disp(['My motory jedeme na ' num2str(j) '. pozici z ' num2str(pocet_mereni_dipu) ])

    for mn=1:2    %1=velky_interf, 2=maly_interf
        fprintf(motorek,[num2str(mn) 'PT' num2str(pojezd(mn,j)) '\n'])
             %vyhodi cas, ktery motor potrbuje pro cestu na pozici j
        pt=fscanf(motorek);
             %vraci odpoved ve tvaru 1PTcislo, kde cislo je trvani pohybu
        delka_pt=length(pt)-2; %delka stringu pt bez konce radku
```

```
        trvani_pohybu=str2num(pt(4:delka_pt));
        fprintf(motorek, [num2str(mn) 'PA' num2str(pojezd(mn,j)) '\n'])
             %motore, jed na pozici "j"
        pause(trvani_pohybu) %cekame, az motor dojede kam ma
    end

%%%%%%%%%%%% 1 mereni 20s dlouhe%%%%%%%%%%%%%%%%%%%%%%%%%%%%%%%%%%%%%%%%%%%%%%%%%
    dip_vektor=[];
    quady_dual_mereni %meri pomoci DUALU A 2 QUADU
    dipV=channel9;
    dipM=channel10;

        if dipV==0
            chyba_dipV=0;
        else
            chyba_dipV=(dipV)^(0.5);
        end

        if dipM==0
            chyba_dipM=0;
        else
            chyba_dipM=(dipM)^(0.5);
        end

    dip_vektor=[ j, velky_m(j), dipV, chyba_dipV, maly_m(j), dipM, chyba_dipM,];
%%%%%%%%%%%%%%%zapis vysledku%%%%%%%%%%%%%%%%%%%%%%%%%%%%%%%%%%%%%%%%%%%%%%%%%%%%%
    dip=[dip; dip_vektor];
    fid=fopen(soubor, 'a');
    fprintf(fid, '%1.0f %3.3f %3.0f %3.3f %3.3f %3.0f %3.3f\n', dip_vektor);
    fclose(fid);

end %for j=1:pocet_mereni_dipu


%%%%%%%%%%%%%% fit %%%%%%%%%%%%%%%%%%%%%%%%%%%%%%%%%%%%%%%%%%%%%%%%%%%%%%%%%%%%%%%%%

%------ vyber potrebnych dat ----------------------------------------------
x_velky = dip(:,2);
y_velky = dip(:,3);

x_maly = dip(:,5);
y_maly = dip(:,6);
%---- fit polynomem 2.stupne ------------------------------------------------
p_velky = polyfit(x_velky,y_velky,2);
f_velky = polyval(p_velky,x_velky);

p_maly = polyfit(x_maly,y_maly,2);
f_maly = polyval(p_maly,x_maly);
        %----- hledej minimum ------------------
        %----- velky interferometr
        av=p_velky(1);
        bv=p_velky(2);
        cv=p_velky(3);

        xx_v=[];yy_v=[];
        xx_v=min(x_velky):0.001:max(x_velky);
        yy_v=av.*(xx_v.^2) + bv.*xx_v + cv;
        min_velky=min(yy_v);
        [m,n]=find(yy_v==min_velky);
        stred_velky=xx_v(n);

        %----- maly interferometr
        am=p_maly(1);
        bm=p_maly(2);
        cm=p_maly(3);
```

```
        xx_m=[];yy_m=[];
        xx_m=min(x_maly):0.001:max(x_maly);
        yy_m=am.*(xx_m.^2) + bm.*xx_m + cm;
        min_maly=min(yy_m);
        [mm,nn]=find(yy_m==min_maly);
        stred_maly=xx_m(nn);
%-------------

        visV=(max(y_velky)-min(y_velky))/(max(y_velky)+min(y_velky))*100
        visM=(max(y_maly)-min(y_maly))/(max(y_maly)+min(y_maly))*100

    minimum_dipu=[den mesic casek stred_velky stred_maly];
    fid1=fopen(soubor1, 'a');
    fprintf(fid1, '%2.0f %2.0f %3.3f      %3.3f %3.3f \n', minimum_dipu );
    fclose(fid1);

%------ vykresleni ------------------------------------------------------
figure
plot(x_velky, y_velky , 'ro')
hold on
plot(x_maly, y_maly , 'bo')

plot(x_velky, f_velky , '-r')
plot(x_maly, f_maly , '-b')

plot(stred_velky, min_velky , '.k')
plot(stred_maly, min_maly , '.k')
hold off

title(['HOM dip z ' num2str(datum(3)) '.' num2str(datum(2)) '.' num2str(datum(1)) 'v '
num2str(datum(4)) 'h. ' num2str(datum(5)) 'min. cervena-VELKYmin=' num2str(stred_velky)
'mm, modra-MALYmin=' num2str(stred_maly) 'mm'])


%%%%%%%%%%%%nastaveni motoru nas stred dipu%%%%%%%%%%%%%%%%%%%%%%%%%%%%%%%%
fprintf(motorek, ['1PA' num2str(stred_velky) '\n']) %motore, jed na pozici "velky_min"
fprintf(motorek, ['2PA' num2str(stred_maly) '\n']) %motore, jed na pozici "maly_min"

disp(['my motory jedeme na pozice: ' num2str(stred_velky) ' mm velky a maly '
num2str(stred_maly) ' mm -do stredu HOM dipu ' ])
disp(['visibilita HOM dipu:' num2str(visV) ' % velky dip a ' num2str(visM) '% maly dip
' ])

pause(10)
close_motor
```

2. MATLAB routine for the second scan of the HOM dip (see Section 4.2)

```
function [stred_velky, stred_maly, visV,
visM]=promereni_dipu(stred_dipu,delka_scanu,pocet_mereni_dipu,rozsah_min)

porty
casova_zakladna='s';
doba_mereni=1;
pocet_cyklu=1;
inic_counteru
dual_nastaveni
inic_motorecek
inic_karet_dio
test_pruchodnosti_vrtulek
pozice=3;
puls_x
%%%%%%%%%%%%%%%%%%%%%%%%%%%%%%%%%%%%%%%%%%%%%%%%%%%%%%%%%%%%%%%%%%%%5
mereni_dip=linspace(stred_dipu-delka_scanu,stred_dipu+delka_scanu,pocet_mereni_dipu);
dip=[];
date %den, mesic, rok, hodina, minuta
stri='%3.0f';
%%%%%%%%%%%%%%%nastaveni zapisovani vysledku do souboru%%%%%%%%%%%%%%%%%%%%%%
soubor='HOM_dip_zdroj.dat';
fid=fopen(soubor, 'a'); %pripis do puvodni souboru
fprintf(fid, ['\n Mereni HOM dipu z ' num2str(den) '.' num2str(mesic) '.' num2str(rok)
'v ' num2str(hodina) 'h. ' num2str(minuta) 'min. (Pojezd motorem ve zdroji)']);
fprintf(fid, ['\n SOUBOR: poradi, poloha_motor_velky, coinc_velky,
chyba_coinc_velky_dip, poloha_motor_maly, coinc_maly, chyba_coinc_maly_dip' '\n']);
fclose(fid);
soubor1='fit_dip_zdroj.dat'; %koeficienty parabolickeho fitu,1. a 2. linearniho fitu,
krajni intenzita pro parab. fit
soubor2='data_dip.dat'; %data k primemu pouziti
%%%%%%%%%%%%%%%%%%%%%%%%%%%%%%%%%%%%%%%%%%%%%%%%%%%%%%%%%%%%%%%%%%%%%%%%%%%
doba_mereni=150; %JAK DLOUHO SE MERI V 1 BODE DIPU
dual_nastaveni
for j=1:pocet_mereni_dipu
        misto=mereni_dip(j);
        motorecek_misto

%%%%%%%%%%%% 1 nacteni hodnot 20s dlouhe%%%%%%%%%%%%%%%%%%%%%%%%%%%%%%%%%%%%%%%%

        dip_vektor=[]; %slouzi k vyprazdneni predchoziho mereni
        disp([num2str(j) '. mereni.'])
        quady_dual_mereni %meri pomoci DUALU A 2 QUADU
        dipV=channel9;
        dipM=channel10;
    %----------spocteni chyby namerene hodnoty
        if dipV==0
            chyba_dipV=0;
        else
            chyba_dipV=(dipV)^(0.5);
        end

        if dipM==0
            chyba_dipM=0;
        else
            chyba_dipM=(dipM)^(0.5);
        end
    %-----------------------------------------
        dip_vektor=[ j, mereni_dip(j), dipV, chyba_dipV, dipM, chyba_dipM,];
%%%%%%%%%%%%%%%zapis vysledku%%%%%%%%%%%%%%%%%%%%%%%%%%%%%%%%%%%%%%%%%%%%%%%
    dip=[dip; dip_vektor];
    fid=fopen(soubor, 'a');
    fprintf(fid, '%1.0f %3.3f %3.0f %3.3f %3.0f %3.3f\n', dip_vektor);
```

```
    fclose(fid);
%%%%%%%%%%%%%%%%%%%%%%%%%%%%%%%%%%%%%%%%%%%%%%%%%%%%%%%%%%%%%%%%%%%%%%%%%%%%%%%

end %j=1:pocet_mereni_dipu

%%%%%%%%%%%%%% FIT %%%%%%%%%%%%%%%%%%%%%%%%%%%%%%%%%%%%%%%%%%%%%%%%%%%%%%%%%%%
%pouzijeme data z velkeho interf.:

%%%%%%%%%%%%%%% 1 nalezeni minima %%%%%%%%%%%%%%%%%%%%%%%%%%%%%%%%%%%%%%%%%%%
%------ vyber potrebnych dat ------------------------------------------------
disp('Parabolicky fit okoli minima pro nalezeni pozice minima.')
minimum_dip=min(dip(:,3));
[minv]=find(dip(:,3)==minimum_dip); %%nalezeni minima
minv=minv(1);
x_velky = dip(minv-rozsah_min:minv+rozsah_min,2); %polohy v okoli minima
y_velky = dip(minv-rozsah_min:minv+rozsah_min,3); %county v okoli minima

[minm]=find(dip(:,6)==min(dip(:,6))); %%nalezeni minima
minm=minm(1);
x_maly = dip(minm-rozsah_min:minm+rozsah_min,2);
y_maly = dip(minm-rozsah_min:minm+rozsah_min,5);

%---- fit polynomem 2.stupne ---------------------------------------------
p_velky = polyfit(x_velky,y_velky,2);
f_velky = polyval(p_velky,x_velky);

p_maly = polyfit(x_maly,y_maly,2);
f_maly = polyval(p_maly,x_maly);


fid=fopen(soubor1, 'w');
fprintf(fid,'%10f\n', p_velky);
fclose(fid);

%----- hledej minimum ------------------------------------------------
 %velky interferometr
 av=p_velky(1);
 bv=p_velky(2);
 cv=p_velky(3);

 xx_v=min(x_velky):0.001:max(x_velky);
 yy_v=av.*(xx_v.^2) + bv.*xx_v + cv;
 [mv,strv]=min(yy_v); %mv=minimum z yy_v
 stred_velky=xx_v(strv);
 disp(['Dip velkeho interf. ma minimum na pozici ' num2str(stred_velky) 'mm.']);

 %maly interferometr
 am=p_maly(1);
 bm=p_maly(2);
 cm=p_maly(3);

 xx_m=min(x_maly):0.001:max(x_maly);
 yy_m=am.*(xx_m.^2) + bm.*xx_m + cm;
 [mm,strm]=min(yy_m); %mm=minimum z yy_m
 stred_maly=xx_m(strm);
 disp(['Dip maleho interf. ma minimum na pozici ' num2str(stred_maly) 'mm.']);
%---------------------------------
visV=(max(dip(:,3))-min(dip(:,3)))/(max(dip(:,3))+min(dip(:,3)))*100;
visM=(max(dip(:,5))-min(dip(:,5)))/(max(dip(:,5))+min(dip(:,5)))*100;
disp('*')
disp(['Visibilita velkeho interferometru je ' num2str(visV) '%.'])
disp(['Visibilita maleho interferometru je ' num2str(visM) '%.'])
disp('*')
%-----------------------------------
if dip(minv-rozsah_min,3) > dip(minv+rozsah_min,3)
```

```
krajni_int=dip(minv-rozsah_min,3);
else
krajni_int=dip(minv+rozsah_min,3);
end
%%%%%%%%%%%%%% 2 ulozeni linearnich fitu %%%%%%%%%%%%%%%%%%%%%%%%%%%%%%%%%%%%%%%
%pouziva se pro korekci poloh odpovidajicich ruznym bodum v dipu (viz HLAVNI_PROGRAM)
%fitujeme mezi 0.1 a 0.8 * (max(koinc)-min(koinc))
disp('Vypocet linearnich fitu pro steny dipu.')
max_dipu=max(dip(:,3)); max_dipu=max_dipu(1); %osetreni vuci pripadu dvou stejnych
maxim
hranice=[0.15*max_dipu 0.8*max_dipu];
max_int_prava=max(dip(minv:pocet_mereni_dipu,3));
[max_dipu_prava]=find(dip(:,3)==max_int_prava);
[max_dipu_leva]=find(dip(:,3)==max(dip(1:minv,3)));
pozice_maxima=dip(max_dipu_prava,2);

for q=1:2
hledani_leva=abs(dip(max_dipu_leva:minv,3)-hranice(q)); %fit pro levou stranu dipu
hledani_prava=abs(dip(minv:max_dipu_prava,3)-hranice(q)); % fit pro pravou stranu dipu
eval(['[indi' num2str(q) '_leva]=find(hledani_leva==min(hledani_leva));'])
eval(['[indi' num2str(q) '_prava]=find(hledani_prava==min(hledani_prava));'])
end
inx_hr=[max_dipu_leva-1+indi2_leva max_dipu_leva-1+indi1_leva; minv-1+indi1_prava minv-
1+indi2_prava];
hranice=[dip(inx_hr(2),3) dip(inx_hr(1),3); dip(inx_hr(3),3) dip(inx_hr(4),3)];

x_lin_L=dip(inx_hr(1,1):inx_hr(1,2),2);
y_lin_L=dip(inx_hr(1,1):inx_hr(1,2),3);
x_lin_P=dip(inx_hr(2,1):inx_hr(2,2),2);
y_lin_P=dip(inx_hr(2,1):inx_hr(2,2),3);
linL=polyfit(x_lin_L,y_lin_L,1); %fit pro levou stranu dipu, leva_lin(1)=koeficient u
x^1, leva_lin(21) u x^0
linP=polyfit(x_lin_P,y_lin_P,1); % fit pro pravou stranu dipu
leva_lin=polyval(linL,x_lin_L);
prava_lin=polyval(linP,x_lin_P);
slope_L=linL(1);
slope_P=linP(1);
%spocteni mista nejvyssi derivace (pouzivame jen pravou stranu dipu):
pul_int=(mean(dip((max_dipu_prava+5):pocet_mereni_dipu,3)))/2; %polovicni intenzita
vzhledem k maximu mimo usi dipu
chyba_pul_int=sqrt(pul_int);
hledani=abs(dip(minv:max_dipu_prava,3)-pul_int);
indi=find(hledani==min(hledani));
x_pul_int=dip(minv-1+indi,2); %poloha mista nejvetsi derivace (prava strana)
%zapis pro pouziti v hlavnim programu:
fid=fopen(soubor1, 'a');
fprintf(fid, '%10f\n', linP, linL);
fprintf(fid, '%10f\n', krajni_int); %krajni intenzita parabol. fitu kolem minima
fclose(fid);

%%%%%%%%%%%%%% grafy %%%%%%%%%%%%%%%%%%%%%%%%%%%%%%%%%%%%%%%%%%%%%%%%%%%%%%%%%%

figure, plot(dip(:,2),dip(:,3))
hold on, plot(xx_v, yy_v,'r')
hold on, plot(x_lin_L,leva_lin,'g*-')
hold on, plot(x_lin_P,prava_lin,'g*-')
hold off

figure, plot(dip(:,2),dip(:,5))
hold on, plot(xx_m,yy_m,'r')

%--------------------
figure, plot(dip(:,2),dip(:,3), '-ro')
hold on, plot(dip(:,2),dip(:,5), '-bo')
hold off
```

```
title(['HOM DIP inteferom... cervene-VELKY vis= ' num2str(visV) '%, modre-MALY vis='
num2str(visM) ])

pif_maxV=max(dip(:,3));
pif_maxM=max(dip(:,5));
figure, plot(dip(:,2),dip(:,3)/pif_maxV, '-ro')
hold on, plot(dip(:,2),dip(:,5)/pif_maxM, '-bo')
hold off
title(['HOM DIP normovany inteferom... cervene-VELKY vis= ' num2str(visV) '%, modre-
MALY vis=' num2str(visM) ])
%%%%%%%%%%%%%%% zapis dat k primemu pouziti %%%%%%%%%%%%%%%%%%%%%%%%%%%%%%%

fid=fopen(soubor2, 'w');
fprintf(fid,'%4.0f %3.0f %6.3f %2.0f %6.3f %4.0f %3.0f %6.3f\n', pul_int,
chyba_pul_int, x_pul_int, doba_mereni, stred_velky, max_int_prava, minimum_dip,
pozice_maxima);
fclose(fid);
%%%%%%%%%%%nastaveni motoru na stred dipu%%%%%%%%%%%%%%%%%%%%%%%%%%%%%%%%%
disp('Motor jede na zacatek.')
misto=stred_dipu-delka_scanu;
motorecek_misto
pause(5)
disp(['Motor jede do minima dipu: ' num2str(stred_velky) 'mm.'])
misto=stred_velky;
motorecek_misto
%%%%%%%%%%% konec mereni %%%%%%%%%%%%%%%%%%%%%%%%%%%%%%%%%%%%%%%%%%%%%%%%%
close_motorecek
zavreni_counteru
```

3. MATLAB routine for the main measurement

```
function HLAVNI_PROGRAM(pocet_poloh_dip, pocet_fazi, delici_pomer, pocet_cyklu_pary,
interf)
%%%%%%%%%%%%%%%%%%%%%%%%%%%%%%%%%%%%%%%%%%%%%%%%%%%%%%%%%%%%%%%%%%%%%%%%%%%%%%%%%%%
%program meri koincidencni raty pro pocet_poloh_dip ruznych poloh dipu a pocet_fazi
fazi program. qubitu
%pozn. pred spustenim programu je treba rucne nastavit out VRC (if applicable) a
spustit program na nastaveni minim dipu
%delici_pomer=50 - 50:50, delici_pomer=100 - 0:100
%merime pro 7 hodnot fazi prg qubitu

casova_zakladna='s';
doba_mereni_PROBE=0.1; %0.1;    %sekundy
doba_mereni_PARY=3;             %3s
doba_mereni_DIP=100;
doba_mereni_vrtule=1;
addpath('stab') %propojeni se slozkou obsahujici programy pro stabilizaci
porty
spatne=0;
hystereze_motorecku=0.2;
if delici_pomer==50
max_faze_out=1;
elseif delici_pomer==100
max_faze_out=0;
else
disp('Zadejte spravne delici pomer (50 nebo 100).')
error('Spust znova.')
end
%-------------------------------------inicializace-------------------------------
inic_karet_analog  %vytvori objekt ao pro komunikaci s kartami a viktora_napeti [0 0 0
0 0] V
inic_karet_dio %vytvori objekt dio na komunikaci s kartou a vytvori vektora_dio [0 0 0
0] V
inic_counteru  %Q2ext_D1 - inicializuji se QUADY s externi casovou zakladnou a DUAL
inic_motorecek

%viktor_napeti=[PM_stab_maly, PM_stab_velky]
% viktor_naperi(vik) - "vik"-tá složka vektoru
% i=1; %PM_stab_VELKY+faze_OUT
% i=2; %PM_stab_maly+faze_prog_qubitu - pri nastaveni merici baze=0, meni
% se samostatnym prikazem
%vrtulky:
%vrt. c. 3- zakryva cervenou diodu
%vrt. c. 4- zakryva modry laser
%-------------------------------------ukladani do souboru-------------------------
date_string
ukladani=['wm1-100bezFF' rok mesic den '.dat'];
fid=fopen(ukladani, 'a');
fprintf(fid,['\n#Mereni z ' den '.' mesic '.' rok ' v ' hodina 'h ' minuta 'min.\n']);
fprintf(fid,['#Koincidencni mereni ve ' num2str(pocet_poloh_dip) ' ruznych polohach
dipu a pro ' num2str(pocet_fazi) ' ruznych fazi programoveho a datoveho qubitu.\n']);
fprintf(fid,['#Pro kazdou fazi se provadi sady ' num2str(pocet_cyklu_pary) '-ti mereni
po ' num2str(doba_mereni_PARY) 's.\n']);
fprintf(fid,['#Delici pomer out: ' num2str(delici_pomer) ' \n']);
fprintf(fid, ['#SOUBOR: (1-2)intenzitni pozice dipu, pozadovana a realna, (3)poloha
motoru v mm, (3)faze prog. qubitu, (4) faze dat. qubitu,\n'])
fprintf(fid,['#(5) faze out, (6) delici pomer out, (7-10)singly velky a maly resp.,
(11-14)krizove koinc, (15-16)koincidence dipu, velkeho a maleho resp., (17-18)absolutni
hodnota maxima L1-L2, S1-S2 merena '  num2str(doba_mereni_DIP) ' s\n']);
fprintf(fid, ['#Pozn.: Mereni se zmenou faze dat. a prf. qubitu jsou pro prehlednost
oddelena mezerou.\n\n']);
% fprintf(fid, ['#Pozn.: faze v souboru je udavana ve stupnich, 0-180°.\n']);
fclose(fid);
```

```
prepis_int='max_int.dat';
%-----------------------------------nastaveni-----------------------------------------
 doba_mereni=doba_mereni_vrtule; %sekundy
 dual_nastaveni
 det_ucinnosti; %nacteni detekcnich ucinnosti APD
%---------------------testy pruchodnosti-------------------------------------------
 pause(0.5)
 %predpoklada se, ze flipy jsou otevrene na pruchod - jde to videt okem
 test_pruchodnosti_vrtulek  %nastavi obe VRTULKY tak tak, aby propoustely fotony signal
i idler do experimentu
 pozice=3; %PARY (modry laser) odkryte, PROBE (cerveny laser) zakryty
%  pozice=4; %PROBE (cerveny laser) odkryty, PARY (modry laser) zakryte
 puls_x

%-------------------------nacteni pozadi-------------------------------------------
pozadi = dlmread('pozadi_a_temne.dat');  % nacte predem namerene pozadi vcetne temnych
countu
%----------------------nacteni pulvlnnych napeti-----------------------------------
pulvlnna_napeti;          %obsahuje pluvlnna napeti jednotlivych PM

%------------------------nacteni parametru pro mereni---------------------------------
% stredy_dipu=dlmread('minima_HOM_dipu.dat');
fit_dip=importdata('fit_dip_zdroj.dat'); %vektor fit_dip 1-3: parabolicky fit v okoli
minima, 4-5 lin. fit leva strana, 6-7 lin. fit prava strana, 8 krajni intenzita
parabol. fitu kolem minima
data_dip=importdata('data_dip.dat');
%------------------------soubory na ukladani dat---------------------------------------
%------------------------MERENI-------------------------------------------------------
%-----------------------parametry mereni-----------------------------------------
kroku_napeti=70;         %k mereni visibility a pro stabilizaci
max_pocet_stab_cyklu=5;  %ke stabilizaci

%-----------------------info o dipu-----------------------------------
x_pul_int=data_dip(3); %poloha mista nejvetsi derivace
doba=data_dip(4);
pul_int_st=data_dip(1); %velikost polovicni intenzity (pocet koincidenci v miste
nejvetsi derivace)
max_int_st=2*pul_int_st;
krajni_int=fit_dip(8);
stred_velky=data_dip(5);
minimum_dip=data_dip(7);
pozice_maxima=data_dip(8);
if delici_pomer==100
   max_int=prepis_int(1);
   max_int_maly=prepis_int(2);
   delta_x=prepis_int(3);
   korekce_max=max_int_st/max_int; %korekce vuci kolisani intenzity
end
delta_x=0;
%-------------------------------------------------------------------------------
% TADY: for d=1:1-meri se1.bod dipu, for d=2:2-meri se2.bod dipu..atp
for d=1:pocet_poloh_dip %meri se v minimu, maximu, a v pocet_poloh_dip-2 dalsich
polohach mezi
    %d=1:pocet_poloh_dip

    %-------------------------mereni pro overeni pozice dipu---------------------
    disp([num2str(d) '. POLOHA V DIPU z celkem ' num2str(pocet_poloh_dip) ' poloh'])
    %mer v polovine
    pocet_cyklu=1;

  if delici_pomer==50
    doba_mereni=doba_mereni_DIP;
    dual_nastaveni
    disp('Mereni intenzity mimo dip - max. intenzity.')
    disp('Pojezd motoru kvuli pripadne hysterezi.')
```

```
    misto=pozice_maxima-delta_x+0.3-hystereze_motorecku;
    motorecek_misto;
    misto=pozice_maxima-delta_x+0.3; %pozice se prubezne posouva s dipem pomoci
kumulovaneho delta_x
    motorecek_misto;
    quady_dual_mereni  %meri pomoci DUALU A 2 QUADU
    max_int=channel9;
    max_int_maly=channel10;
    disp(['Maximalni intenzita: ' num2str(max_int)])
    chyba=sqrt(max_int);
    interval=2*chyba;
    disp(['Tolerance ' num2str(interval) '.'])
    %zapis max.int
    fid=fopen(prepis_int,'w');
    fprintf(fid,'%4.0f %4.0f',max_int, max_int_maly);
    fclose(fid);
    korekce_max=max_int_st/max_int; %korekce vuci kolisani intenzity
    %------------
    kolisani=max_int/2-(pul_int_st/doba)*doba_mereni;
    disp('Stara polovicni intenzita:')
    disp([num2str((pul_int_st/doba)*doba_mereni)]);disp('');
    disp('Nynejsi polovicni intenzita:')
    pul_int=max_int/2;
    disp([num2str(pul_int)]);
    disp('Kolisani intenzity:')
    disp([num2str(kolisani)]);
    disp('Pojezd motoru kvuli pripadne hysterezi.')
    misto=x_pul_int-delta_x-hystereze_motorecku;
    motorecek_misto;
    disp('Mereni v 1/2 normovane intenzity dipu (misto nejvetsi derivace).')
    misto=x_pul_int-delta_x; %pozice se prubezne posouva s dipem pomoci kumulovaneho
delta_x
    motorecek_misto;   %motor jede na pozici "misto"
    quady_dual_mereni  %meri pomoci DUALU A 2 QUADU
    I1=channel9;
    disp(['V miste 1/2 intenzity bylo za ' num2str(doba_mereni) 's namereno:'])
     disp([num2str(I1) ' countu'])
    %-----------------------overeni pozice dipu a najeti na pozadovane misto-----------
    korekce=0;
    if (I1>(pul_int+interval) | I1<(pul_int-interval)) && d~=pocet_poloh_dip
        while ((I1>(pul_int+interval) | I1<(pul_int-interval))) && korekce<=1
        %pokud neni v intervalu, spocitej posuv
        disp('Dip ujel. Probiha korekce.')
        delta_x=delta_x+((I1-pul_int)*korekce_max)/fit_dip(4); %musime normovat
vzhledem k dobe mereni platne pro fit
        disp('Pojezd motoru kvuli pripadne hysterezi.')
        misto=x_pul_int-delta_x-hystereze_motorecku; %kvuli pripadne hysterezi
        motorecek_misto
        misto=x_pul_int-delta_x; %pozn. slope is always positive (prava strana dipu)
        motorecek_misto; %najed do pozice
        quady_dual_mereni %mer znovu
        I1=channel9;
        disp(['V miste 1/2 intenzity bylo po korekci (za ' num2str(doba_mereni) 's)
namereno:'])
         disp([num2str(I1) ' countu'])
        fid=fopen(prepis_int,'a');
        fprintf(fid,' %7.3f',delta_x);
        fclose(fid);
     if I1>(pul_int+interval) | I1<(pul_int-interval)
        disp('Dip ujel a korekce nezafungovala.')
        korekce=korekce+1;
     end

        end %while
    else
```

```
        delta_x=delta_x+0;
    end % if I1 nespada do tolerancniho intervalu

  end %delici_pomer==50

%%%%%%%%%%%%%%%%%%%vypocet pozice mista v dipu%%%%%%%%%%%%%%%%%%%

            int_poloha=(d-1)*(max_int/(pocet_poloh_dip-1));
            if int_poloha==0
               misto_int=stred_velky-delta_x; %abychom se vyhli komplexnim cislum
            elseif abs(int_poloha-max_int) <= (max_int*0.0002)%abychom se vyhli usim,
kde nevime, co se tam presne deje
               misto_int=stred_velky-delta_x+0.3;
            else
                if int_poloha <= (krajni_int/doba)*doba_mereni
                %pouzij parabol. fit
                %int_poloha*korekce_max=fit_dip(1)*x^2+fit_dip(2)*x+fit_dip(3)
                delta=fit_dip(2)^2-4*fit_dip(1)*(fit_dip(3)-(int_poloha*korekce_max));
                misto_int=((-fit_dip(2)+sqrt(delta))/(2*fit_dip(1)))-delta_x;
                else
                %pouzij lin. fit na prave strane dipu
                misto_int=((int_poloha*korekce_max-fit_dip(5))/fit_dip(4))-delta_x;
                end
            end

relativni_int=int_poloha/max_int;
disp(['Najeti do mista ' num2str(relativni_int*100) '% intenzity dipu.'])

disp('Pojezd motoru kvuli pripadne hysterezi.')
misto=misto_int-hystereze_motorecku; %kvuli pripadne hysterezi
motorecek_misto
misto=misto_int;
motorecek_misto
if delici_pomer==50
quady_dual_mereni
I1=channel9;
real_int=channel9/max_int;
disp(['Realna intenzita je vsak: ' num2str(real_int*100) '%.'])
elseif delici_pomer==100
    real_int=0;
end
%----------------------mereni pro ruzne faze-------------------------
%mereni visibility pred samotnym merenim - pro %stabilizaci
if delici_pomer==50
probe
mereni_visibilit
pary
end
for faze_out=0:max_faze_out %v jedne poloze v dipu se meri nejprve s fazi_out=0°, pote
s fazi_out=90°
    %faze_out=0 - nenastavujeme fazi pro vystupni bazi, faze_out=1 - meri
    %se v bazi s fazi pi (tj. baze |0>+-i|1>)
    faze_out_stupne=faze_out*90;

  for qu=1:2
faze_qubitu=0:1/(pocet_fazi-1):1;
faze_qubitu(2:pocet_fazi-1)=faze_qubitu(2:pocet_fazi-1)*(-1)^qu;
qubit=[0 0];
    for f=1:pocet_fazi

                for cykl=1:pocet_cyklu_pary
                    if delici_pomer==50
                    probe %nastaveni na pruchod diody a zacloneni paru
                    STABILIZACE
                    pary %nastaveni na pruchod paru a zacloneni diody
```

```
                    elseif delici_pomer==100
                    doba_mereni=doba_mereni_PARY;
                    dual_nastaveni
                    end
                nastaveni_faze
                faze=faze_qubitu(f)*180;
                qubit(qu)=faze;
                quady_dual_mereni2  %meri pomoci DUALU A 2 QUADU, bez poctu cyklu
uvnitr, kvuli prubeznemu zapisovani
                disp('tydli tydli')
                %--------------------prubezne ukladani vysledku--------------------
                fid=fopen(ukladani,'a');
                fprintf(fid,'%0.4f; %0.4f; %2.3f; %3.0f; %3.0f; %3.0f; %3.0f; ',
relativni_int, real_int, misto, qubit(1), qubit(2), faze_out_stupne, delici_pomer);
                fprintf(fid,'%5.0f; %5.0f; %5.0f; %5.0f; %5.0f; ', channel1, channel2,
channel3, channel4, channel5);
                fprintf(fid,'%5.0f; %5.0f; %5.0f; %5.0f; %5.0f; %5.0f; %5.0f',
channel6, channel7, channel8, channel9, channel10, max_int, max_int_maly);
                fprintf(fid,'\n');
                fclose(fid);
                %------------------------------------------------------------
                odebrani_faze
                end %cykl=1:pocet_cyklu_pary

    end %f=1:pocet_fazi
    fid=fopen(ukladani,'a');
    fprintf(fid,'\n');
    fclose(fid);
  end %for qubit

 end
end %for pocet_poloh_dip

disp('Konec mereni. Success!')
zavreni_counteru
zavreni_karet
close_motorecek

end
```

4. Photograph of the experiment.

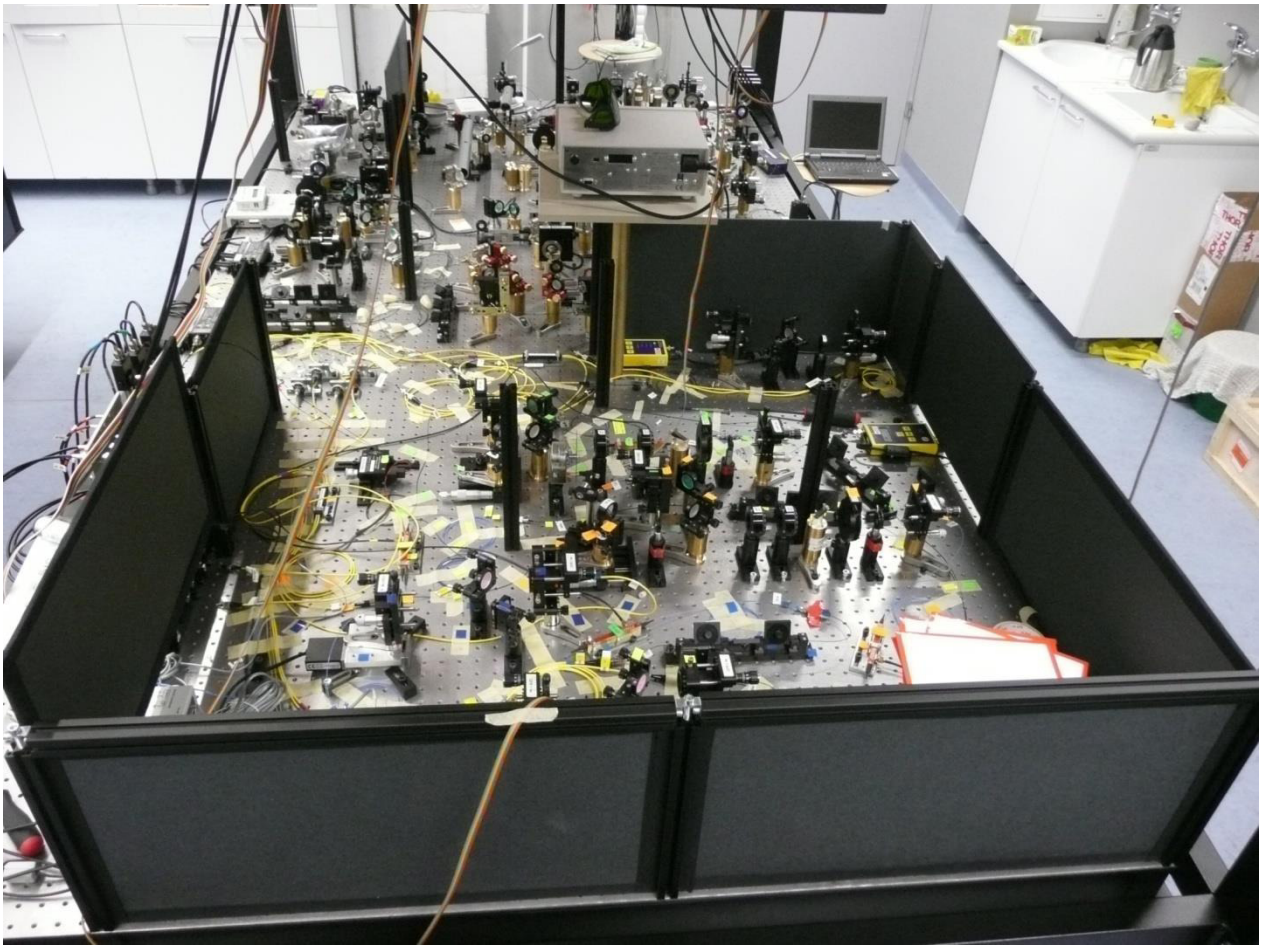

5. Detailed scheme of the setup.